Author for correspondence:
A. Nobili
e-mail: andrea.nobili@unimore.it

A new Rayleigh-like wave in guided propagation of antiplane waves in couple stress materials

A. Nobili[1,3], E. Radi[2,3] and C. Signorini[3]

[1]Department of Engineering Enzo Ferrari, University of Modena and Reggio Emilia, via Vivarelli 10, 41125 Modena, Italy
[2]Department of Sciences and Methods of Engineering, University of Modena and Reggio Emilia, via Amendola 2, 42122 Reggio Emilia, Italy
[3]Centre En&Tech, p.le Europa 1, 42124 Reggio Emilia, Italy

(iD) AN, 0000-0002-9657-5903

Motivated by the unexpected appearance of shear horizontal Rayleigh surface waves, we investigate the mechanics of antiplane wave reflection and propagation in couple stress (CS) elastic materials. Surface waves arise by mode conversion at a free surface, whereby bulk travelling waves trigger inhomogeneous modes. Indeed, Rayleigh waves are perturbations of the travelling mode and stem from its reflection at grazing incidence. As is well known, they correspond to the real zeros of the Rayleigh function. Interestingly, we show that the same generating mechanism sustains a new inhomogeneous wave, corresponding to a purely imaginary zero of the Rayleigh function. This wave emerges from 'reflection' of a bulk standing mode: This produces a new type of Rayleigh-like wave that travels *away from*, as opposed to along, the free surface, with a speed lower than that of bulk shear waves. Besides, a third complex zero of the Rayleigh function may exist, which represents waves attenuating/exploding both along and away from the surface. Since none of these zeros correspond to leaky waves, a new classification of the Rayleigh zeros is proposed. Furthermore, we extend to CS elasticity Mindlin's boundary conditions, by which partial waves are identified, whose interference lends Rayleigh–Lamb guided waves. Finally, asymptotic analysis in the thin-plate limit provides equivalent one-dimensional models.

1. Introduction

The discovery of surface waves by Lord Rayleigh [1] revealed that bulk waves may interact with a free surface to produce a substantially different type of wave, that still propagates along the surface and yet it decays exponentially in the interior. The recognition of surface waves came timely, for it explained the large vertical tremors (ground roll) that could be clearly identified in those early days of seismogram recording. Yet, as pointed out in [2], large low-frequency horizontal vibrations, similar in nature to Rayleigh waves, appear in seismograms, which can be only explained, within the classical theory, assuming a layered (inhomogeneous) structure for the Earth. Indeed, [3] shows "how the layering in the earth affects surface waves far more strongly than it does body waves" [2, §2.9]. Consequently, one is led to understand that horizontally and vertically polarized surface waves are fundamentally different in nature, for the former are an outcome of the double boundary, while the latter are embedded in the mechanics of wave reflection at a surface [4].

Although this might well be the situation in classical elasticity (CE), the recent discovery that antiplane surface waves are supported by the indeterminate couple stress (alias constrained micropolar) theory suggests that horizontally polarized surface waves may also be incorporated in the theory of surface reflection [5,6]. Immediately, the question arises with regard to what specific feature of the theory is required for that to be the case. In fact, shear horizontal surface acoustic waves are also retrieved in the context of the complete Toupin–Mindlin gradient theory, that involves five microstructural parameters, although they are no longer supported by the simplified version of gradient isotropic elasticity [4]. In [7], the appearance of shear horizontal (SH) surface waves is interpreted as a general perturbation (relaxation) of the CE boundary conditions, which binds 'otherwise essentially skimming bulk SH waves to the limiting surface'. To the same effect, several approaches are possible: from material inhomogeneity to surface periodicity (grating), from multiple interfaces (layering) to magneto-elastic coupling. A combination of the above is considered in [8], dealing with piezoacoustic (Bleustein–Gulyaev) SH surface waves in a functionally graded material (FGM).

This notwithstanding, no study appears in the literature investigating the mechanics of surface reflection in the presence of SH surface waves, in an attempt to single out the characteristic feature that triggers their appearance. This analysis is most easily carried out in the context of the indeterminate couple stress (CS) theory, that is perhaps the simplest strain-gradient theory [9–11]. Indeed, for isotropic materials, it introduces, alongside the classical Lamé moduli, two extra elastic constants, which incorporate the role of the microstructure, for a total of four material parameters. In the case of antiplane motion, only three of these really matter, plus the possible contribution of rotational inertia. In contrast to CE, this theory is no longer self-similar and therefore it successfully predicts some important observable phenomena, such as dispersion of bulk and surface waves [6,12] and size effects [13,14].

A number of contributions have appeared in the literature investigating wave propagation in CS materials. In their pioneering work [15], Graff and Pao consider wave reflection and propagation in the sagittal plane (i.e. plane-strain) of an isotropic CS half-space, in the absence of rotational inertia. In particular, study of mode conversion at a free surface 'is found to be more complicated because of the existence of three types of waves'. Even greater complexity is recently encountered in [16], dealing with wave reflection in the context of plane-strain propagation within gradient isotropic elasticity. Indeed, although the simplified version of the theory is considered, four different waves are triggered upon reflection. In [17], sagittal guided wave propagation in a plate (Rayleigh–Lamb waves) made of isotropic CS material is investigated, in the absence of rotational inertia, and dispersion relations are obtained. Very recently, dispersion of Rayleigh–Lamb waves within three CS theories, including indeterminate CS, was analysed in [18]. [12] studies propagation of Rayleigh waves in the sagittal plane for CS materials in the absence of rotational inertia. A similarity between Rayleigh wave dispersion in CS materials and in lattice structures is pointed out in [19]. Steady-state mode III fracture propagation is considered in [20], which extends the results already obtained in [13] for statics and shows the dispersion diagram of

bulk SH waves. Scattering of antiplane shear waves at the interface of a cylindrical nano-fibre in CS materials is investigated by [21]. Diffraction of waves originating from time harmonic loading of a semi-infinite crack is discussed in [6].

In this paper, we extend the work of Graff and Pao to antiplane waves and upon this we develop the theory of surface and Rayleigh–Lamb antiplane waves in CS materials. With respect to the original work of Graff and Pao, the mechanical framework is simpler and thus we can develop full analytical insight. Besides, the important role of microstructure inertia is assessed. In the process, we discover analogies and differences with sagittal plane propagation in CE. In particular, a standing horizontally polarized bulk wave, associated to a purely imaginary branch-point in the Rayleigh function, takes the place of the familiar longitudinal P-wave in sagittal plane propagation of CE (§3). Still, its role is essential in coupling with the bulk travelling SH-wave at the free surface to produce the antiplane surface wave, much like P and shear vertical (SV) waves couple in CE to produce Rayleigh waves (§3b). Indeed, Rayleigh waves arise in CE at grazing incidence, beyond the critical angle that is attached to reflected P waves being converted into surface waves. Such surface waves are precisely the form in which standing bulk waves appear at the free surface of CS materials. Interestingly, we investigate a novel type of 'reflection' that involves standing waves and leads to a new Rayleigh-like wave, propagating in the interior of the material and exponentially exploding/decaying along the surface (§3c). Clearly, this wave cannot exist on an infinite surface. However, it is precisely this wave, associated with a purely imaginary zero of the Rayleigh function, that is found in [6] radiating from the tip of a semi-infinite crack. Guided propagation in a plate is investigated in §4, where reduced one-dimensional models for beams with microstructure are also obtained.

2. Antiplane couple stress elasticity

Let us consider a Cartesian co-ordinate system (O, x_1, x_2, x_3) and a thin plate $\mathcal{B}_0 = \{(x_1, x_2, x_3) : -h < x_2 < h\}$ made of isotropic elastic couple stress (CS) material, figure 1. This is a polar material, for which, alongside the classical Cauchy stress tensor t, we define the couple stress tensor μ such that, for any surface of unit normal n, it determines the internal reduced couple vector $q = \mu n$ acting across that surface. It is expedient to decompose the Cauchy stress tensor t into its symmetric and skew-symmetric parts, respectively σ and τ,

$$t = \sigma + \tau, \quad \sigma = \mathrm{Sym}\, t, \quad \tau = \mathrm{Skw}\, t. \tag{2.1}$$

In addition, the couple stress tensor μ is split into its deviatoric and spherical parts

$$\mu = \mu^D + \mu^S, \quad \mu^S = \tfrac{1}{3}(\mu \cdot \mathbf{1})\mathbf{1}, \tag{2.2}$$

where $\mathbf{1}$ is the identity tensor and $\cdot$ denotes the scalar product, i.e. componentwise $A \cdot B = A_{ij}B_{ij}$ and Einstein's summation convention on twice repeated subscripts is assumed. According to the principle of virtual work [11,12], one has

$$W = \int_{\mathcal{B}} (\sigma \cdot \mathrm{grad}^T u + \mu \cdot \mathrm{grad}^T \varphi)\, dV, \tag{2.3}$$

where u and φ are, respectively, the displacement and micro-rotation vector fields, while the superscript T denotes the transposed tensor. Unlike Cosserat micro-polar theories, for which displacements and micro-rotations are independent fields, CS theory relates one to the other, through [11, eqn (4.9)]

$$\varphi = \tfrac{1}{2}\,\mathrm{curl}\,u. \tag{2.4}$$

Component-wise, this is $\varphi_i = \frac{1}{2}\mathbb{E}_{ijk}u_{k,j}$, where $\mathbb{E}$ is the rank-3 alternator tensor. Hereinafter, a subscript comma denotes partial differentiation, e.g. $(\mathrm{grad}\, u)_{kj} = u_{k,j} = \partial u_k / \partial x_j$. Thus, we speak of
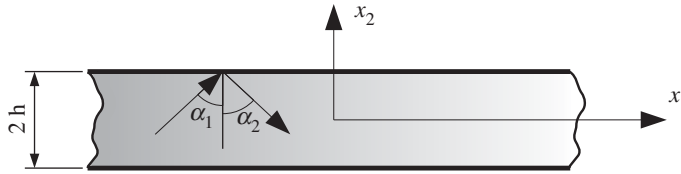
Figure 1. Wave propagation in a homogeneous plate of couple stress elastic material.

latent micro-structure, for micro-rotations are induced by the displacement field. As in CE, we define the linear strain tensor

$$\boldsymbol{\varepsilon} = \text{Sym grad } \boldsymbol{u} \tag{2.5}$$

and thereby observe that, according to (2.3), $\boldsymbol{\sigma}$ is work-conjugated to $\boldsymbol{\varepsilon}$. Further, we introduce the *torsion-flexure (wryness) tensor*

$$\boldsymbol{\chi} = \text{grad } \boldsymbol{\varphi}, \tag{2.6}$$

that, in light of the connection (2.4), is purely deviatoric, i.e. $\boldsymbol{\chi} = \boldsymbol{\chi}^D$. Consequently, to any effect, $\boldsymbol{\mu}$ may be replaced by $\boldsymbol{\mu}^D$ in equation (2.3). Indeed, the CS theory is named indeterminate after the observation that the first invariant of the couple stress tensor, i.e. tr $\boldsymbol{\mu} = \boldsymbol{\mu} \cdot \mathbf{1} = \mu_{11} + \mu_{22} + \mu_{33}$, rests indeterminate and therefore it may be set equal to zero without loss of generality. Therefore, $\boldsymbol{\mu}$ collapses on $\boldsymbol{\mu}^D$ and it is work conjugated with $\boldsymbol{\chi}^T$ [11, eqn (2.22)]. For the sake of brevity, in the following we shall write $\boldsymbol{\mu}$, with the understanding that $\boldsymbol{\mu}^D$ is meant.

Within the framework of hyperelastic materials, the total strain $\boldsymbol{\varepsilon}$ and the torsion-flexure $\boldsymbol{\chi}$ are connected to the stress and to the couple stress through the constitutive relations [21, eqn (12)]

$$\boldsymbol{\sigma} = \frac{\partial U}{\partial \boldsymbol{\varepsilon}}, \qquad \boldsymbol{\mu} = \frac{\partial U}{\partial \boldsymbol{\chi}},$$

where $U = U(\boldsymbol{\varepsilon}, \boldsymbol{\chi})$ is the stored energy potential. At leading order for small deformations of an isotropic material, we get [11, eqn (4.7)]

$$\boldsymbol{\sigma} = 2G\boldsymbol{\varepsilon} + \Lambda(\boldsymbol{\varepsilon} \cdot \mathbf{1})\mathbf{1}, \qquad \boldsymbol{\mu} = 2G\ell^2 \left(\boldsymbol{\chi}^T + \eta \boldsymbol{\chi} \right), \tag{2.7}$$

where Λ and $G > 0$ take up the role of Lamé moduli, $\ell > 0$ is a characteristic length and $-1 < \eta < 1$ is a dimensionless number similar to Poisson's ratio. The material parameters ℓ and η depend on the microstructure and can be connected to the material characteristic length in bending, ℓ_b, and in torsion, ℓ_t, through

$$\ell_b = \ell/\sqrt{2}, \qquad \ell_t = \ell\sqrt{1 + \eta}. \tag{2.8}$$

Values of ℓ_b and ℓ_t may be found in [22,23] and, as an example, for polyurethane foam we have

$$\ell = 0.462 \,\text{mm}, \qquad \eta = 0.797.$$

The limiting value $\eta = -1$ corresponds to a vanishing characteristic length in torsion, which is typical of polycrystalline metals. Clearly, the definitions (2.8) show that $\ell_t = \ell_b$ for $\eta = -1/2$ and $\ell_t = \ell = \sqrt{2}\ell_b$ for $\eta = 0$, the latter situation being the strain gradient effect considered in [24]. For the limiting value $\eta = 1$, the constitutive equation (2.7) provides a symmetric couple stress tensor and, consequently, the present theory reduces to the modified couple stress theory of elasticity introduced in [25]. Indeed, the modified couple stress theory involves only the material length ℓ, in consideration of the restriction $\ell_b = \ell_t/2 = \ell/\sqrt{2}$.

The equations of motion read, in the absence of body forces,

$$\text{div } \boldsymbol{t} = \rho \ddot{\boldsymbol{u}} \tag{2.9a}$$

and

$$\text{axial } \boldsymbol{\tau} + \text{div } \boldsymbol{\mu} = J\ddot{\boldsymbol{\varphi}}, \tag{2.9b}$$

where ϱ is the mass density and $J \geq 0$ is rotational inertia and a superposed dot denotes time differentiation. Here, $(\text{axial } \boldsymbol{\tau})_i = \mathbb{E}_{ijk}\tau_{kj}$ denotes the axial vector attached to a skew-symmetric

tensor. Equation (2.9*b*) may be solved for $\boldsymbol{\tau}$

$$\boldsymbol{\tau} = \tfrac{1}{2}\mathbb{E}\left(\mathrm{div}\,\boldsymbol{\mu} - J\ddot{\boldsymbol{\varphi}}\right), \qquad (2.10)$$

whence the skew-symmetric part of the total stress tensor $\boldsymbol{t}$ is determined by rotational equilibrium. Clearly, CE is retrieved taking $\ell = 0$ and $J = 0$, for then $\boldsymbol{\mu} = \boldsymbol{\tau} = \boldsymbol{o}$ by equations (2.7) and (2.10). As nicely discussed in [12,16], equation (2.10) is generally not objective, in the sense that, owing to the acceleration term, it does not fulfil the requirement of frame indifference. However, for time-harmonic motion, this issue is of no concern [21].

Under antiplane shear deformations, the displacement field $\boldsymbol{u} = (u_1, u_2, u_3)$ is completely defined by the out-of-plane component $u_3 = u_3(x_1, x_2, x_3, t)$. The non-zero components of the micro-rotation vector, of the strain and of the flexure-torsion tensor become

$$\varepsilon_{13} = \tfrac{1}{2}u_{3,1}, \qquad \varepsilon_{23} = \tfrac{1}{2}u_{3,2}, \qquad (2.11a)$$

$$\varphi_1 = \tfrac{1}{2}u_{3,2}, \qquad \varphi_2 = -\tfrac{1}{2}u_{3,1}, \qquad (2.11b)$$

and

$$\chi_{11} = -\chi_{22} = \tfrac{1}{2}u_{3,12}, \quad \chi_{21} = -\tfrac{1}{2}u_{3,11}, \quad \chi_{12} = \tfrac{1}{2}u_{3,22}. \qquad (2.11c)$$

Consequently, equation (2.9) now read [11, eqns (2.7) and (2.9)]

$$\sigma_{13,1} + \sigma_{23,2} + \tau_{13,1} + \tau_{23,2} = \rho\ddot{u}_3, \qquad (2.12a)$$

$$\mu_{11,1} + \mu_{21,2} + 2\tau_{23} = J\ddot{\varphi}_1 \qquad (2.12b)$$

and

$$\mu_{12,1} + \mu_{22,2} - 2\tau_{13} = J\ddot{\varphi}_2. \qquad (2.12c)$$

The constitutive equations (2.7), in light of the definitions (2.5), (2.6) and with the help of the kinematic relations (2.11), give stress and couple stress in terms of displacement [6]

$$\sigma_{13} = Gu_{3,1}, \qquad \sigma_{23} = Gu_{3,2}, \qquad (2.13a)$$

$$\mu_{11} = -\mu_{22} = G\ell^2(1+\eta)u_{3,12}, \quad \mu_{21} = G\ell^2(u_{3,22} - \eta u_{3,11}) \qquad (2.13b)$$

and

$$\mu_{12} = -G\ell^2(u_{3,11} - \eta u_{3,22}). \qquad (2.13c)$$

We observe that the contribution of Λ is immaterial for antiplane deformations, cf. [24, eqns (8–9)]. Besides, introducing equations (2.11*b*), (2.13) into (2.10) yields

$$\tau_{13} = -\tfrac{1}{2}G\ell^2\hat{\triangle}u_{3,1} + \frac{J}{4}\ddot{u}_{3,1}, \qquad \tau_{23} = -\tfrac{1}{2}G\ell^2\hat{\triangle}u_{3,2} + \frac{J}{4}\ddot{u}_{3,2}, \qquad (2.14)$$

which correspond to eqn (9) of [20]. Here, $\hat{\triangle}$ denotes the two-dimensional Laplace operator in the x_1, x_2 co-ordinates. Plugging equations (2.13*a*) and (2.14) into (2.12*a*) gives, for a homogeneous material,

$$G\left(\tfrac{1}{2}\ell^2\hat{\triangle}\hat{\triangle}u_3 - \hat{\triangle}u_3\right) - \frac{J}{4}\hat{\triangle}\ddot{u}_3 + \rho\ddot{u}_3 = 0. \qquad (2.15)$$

In the static case and in the absence of rotational inertia, we retrieve eqn (18) of [26] and eqn (11) of [24].

At any point of a smooth surface we may specify the *reduced force traction* vector $\boldsymbol{p}$ and the tangential part of the *couple stress traction* vector $\boldsymbol{q}$ [11, eqns (3.5–6)]

$$\boldsymbol{p} = \boldsymbol{t}^T\boldsymbol{n} + \tfrac{1}{2}\,\mathrm{grad}\,\mu_{nn} \times \boldsymbol{n}, \qquad \boldsymbol{q} = \boldsymbol{\mu}^T\boldsymbol{n} - \mu_{nn}\boldsymbol{n}, \qquad (2.16)$$

where we have $\mu_{nn} = \boldsymbol{n} \cdot \boldsymbol{\mu}\boldsymbol{n} = \boldsymbol{q} \cdot \boldsymbol{n}$. The reason why only the tangential part of $\boldsymbol{q}$ may be enforced is discussed in [11,12]. In particular, at the bottom/top plate face $x_2 = \mp h$, it is $\boldsymbol{n} = \pm(0, 1, 0)$ and, according to equation (2.16), the out-of-plane component of the reduced force traction and the in-plane components of the couple stress traction read, respectively,

$$p_3 = \pm\left(t_{23} + \tfrac{1}{2}\mu_{22,1}\right), \quad q_1 = \pm\mu_{21}, \quad q_2 = 0. \qquad (2.17)$$

3. Time-harmonic solutions

We introduce the reference length $\Theta\ell$ and the reference time $T = \ell/c_s$ by which we define the dimensionless co-ordinates $(\xi_1, \xi_2, \xi_3) = (\Theta\ell)^{-1}(x_1, x_2, x_3)$ and the dimensionless time $\tau = t/T$. Here, $c_s = \sqrt{G/\rho}$ is the shear wave speed of classical elastic media and Θ is a convenient scaling parameter to be defined in the following. Besides, we let the dimensionless plate half-thickness $H = h/\ell$. With these definitions, the equilibrium equation (2.15) becomes

$$\triangle\triangle u_3 - 2\Theta^2\triangle u_3 - 2\Theta^4\left(\frac{\ell_0^2}{\Theta^2}\triangle u_{3,\tau\tau} - u_{3,\tau\tau}\right) = 0, \tag{3.1}$$

where $\triangle$ is the two-dimensional Laplace operator in ξ_1 and ξ_2 and we have let the dimensionless parameter [20]

$$\ell_0 = \frac{\ell_d}{\ell}, \quad \text{with } \ell_d = \tfrac{1}{2}\sqrt{\frac{J}{\rho}}.$$

We observe that ℓ_d is proportional to the dynamic characteristic length, $l_d = 2\sqrt{6}\ell_d$, introduced in [21].

Under the time-harmonic assumption and considering straight-crested waves in the sagittal plane (ξ_1, ξ_2), we let

$$u_3 = W(\xi_1, \xi_2)\exp(-i\Omega\tau),$$

independent of ξ_3. Here, i is the imaginary unit and $\Omega = \omega T > 0$ the dimensionless (time) frequency. Then, equation (3.1) yields the bi-harmonic PDE [19, eqn (19)] for the function W:

$$\left[\triangle\triangle - 2\left(1 - \ell_0^2\Omega^2\right)\Theta^2\triangle - 2\Omega^2\Theta^4\right]W = 0. \tag{3.2}$$

This homogeneous equation may be easily factored out

$$(\triangle + \delta^2)(\triangle - 1)W = 0, \tag{3.3}$$

provided that Θ is chosen as to satisfy the bi-quadratic equation

$$2\Omega^2\Theta^4 + 2(1 - \ell_0^2\Omega^2)\Theta^2 - 1 = 0.$$

We select the positive root

$$\Theta^2 = \frac{\sqrt{(1 - \ell_0^2\Omega^2)^2 + 2\Omega^2} - 1 + \ell_0^2\Omega^2}{2\Omega^2} \tag{3.4}$$

and observe that Θ is frequency dependent (figure 2). Indeed, it is a strictly monotonic increasing (decreasing) function of Ω, inasmuch as $\ell_0 \gtrless \ell_{0cr} \equiv 1/\sqrt{2}$, that starts from ℓ_{0cr} at $\Omega = 0$ and asymptotes to $\Theta = \ell_0$ for $\Omega \to +\infty$. In fact, the special case $\ell_0 = \ell_{0cr}$ gives the constant behaviour $\Theta \equiv \ell_{0cr}$. In any case, Θ is a bounded function of Ω. By Vieta's formulae applied to (3.2) and (3.3), we have the connection

$$\delta = 2\delta_{cr}\Theta^2, \quad \text{with } \delta_{cr} = \ell_{0cr}\Omega, \tag{3.5}$$

whence, by equation (3.4), we get

$$\delta = \frac{1}{2\delta_{cr}}\left[\sqrt{(1 - \ell_0^2\Omega^2)^2 + 2\Omega^2} - 1 + \ell_0^2\Omega^2\right]. \tag{3.6}$$
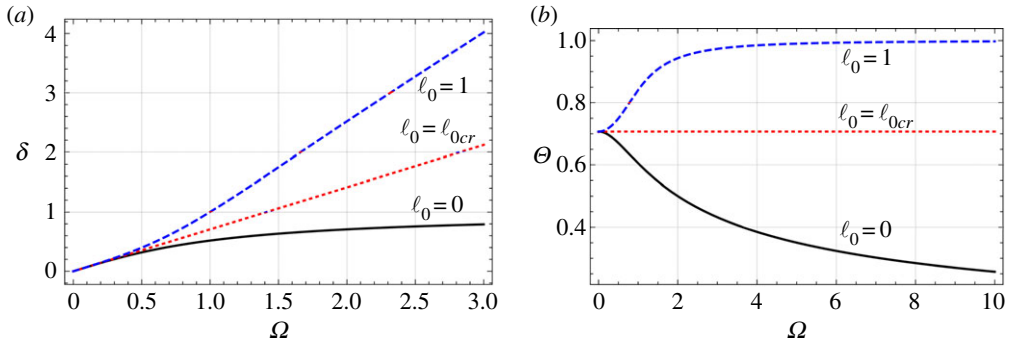
Figure 2. (a) Rescaling parameter Θ and (b) bulk SH wavenumber δ versus Ω at $\ell_0 = 0$ (black, solid), ℓ_{0cr} (red, dotted) and 1 (blue, dashed). (Online version in colour.)

In the special case $\ell_0 = \ell_{0cr}$, it is $\delta = \delta_{cr}$, that is linear in Ω. Figure 2 plots Θ and δ in terms of the dimensionless frequency Ω. We have the asymptotic behaviour for large Ω

$$\delta \sim \begin{cases} 2\ell_0^2 \delta_{cr}, & \ell_0 \neq 0, \\ 1, & \ell_0 = 0, \end{cases} + O(\Omega^{-1}), \quad \text{as } \Omega \to \infty, \tag{3.7}$$

and for small Ω

$$\delta \sim \delta_{cr}, \quad \text{as } \Omega \to 0^+. \tag{3.8}$$

For guided waves propagating along the plate, we have

$$W(\xi_1, \xi_2) = \ell w(\xi_2) \exp(i\kappa \xi_1),$$

where $K = k\ell$ denotes the dimensionless (spatial) wavenumber in the propagation direction ξ_1 and we let the shorthand $\kappa = \Theta K$. Letting $V = \Omega/K$, the dimensionless phase speed along ξ_1, we get that

$$c = \frac{\omega}{k} = Vc_s,$$

is the dimensional phase speed in the propagation direction. Similarly, we take

$$p_3(\xi_1, \xi_2, \xi_3, \tau) = Gt(\xi_2) \exp i(\kappa \xi_1 - \Omega \tau)$$

and

$$q_1(\xi_1, \xi_2, \xi_3, \tau) = G\ell m(\xi_2) \exp i(\kappa \xi_1 - \Omega \tau).$$

The general solution of equation (3.3) is given by

$$w(\xi_2) = \cosh(\lambda_1 \xi_2) e_1 + \cosh(\lambda_2 \xi_2) e_2 + \lambda_1^{-1} \sinh(\lambda_1 \xi_2) o_1 + \lambda_2^{-1} \sinh(\lambda_2 \xi_2) o_2, \tag{3.9}$$

where the wavenumbers in the thickness direction ξ_2 are $\imath \lambda_{1,2}$, with

$$\lambda_1 = \sqrt{\kappa^2 - \delta^2}, \qquad \lambda_2 = \sqrt{\kappa^2 + 1}. \tag{3.10}$$

Branch cuts are taken as to warrant a positive real part for the square root on the real axis, see [6]. The solution (3.9) produces plane bulk waves upon looking for the roots of $\lambda_{1,2} = 0$. In fact, according to this definition of bulk waves, the wavenumber κ is a branch-point of the Rayleigh function and, therefore, a multiple root (here a double root) of the characteristic equation. Consequently, the general form of a bulk wave is given by superposition of a homogeneous with

an inhomogeneous mode, with linearly varying amplitude. The real solution $\kappa = \delta$ corresponds to SH travelling waves moving with phase speed

$$V_{SH} = \frac{\Omega \Theta}{\delta} = \frac{1}{\sqrt{2}\Theta} = \sqrt{\frac{\delta_{cr}}{\delta}}. \qquad (3.11)$$

The purely imaginary solution $\kappa = \iota$ corresponds to a bulk evanescent mode. We name *evanescent* any harmonic solution (mode) whose wavevector has complex-valued components, as opposed to *travelling* modes for which the wavevector is real. Inhomogeneous waves that possess an exponentially varying amplitude are special evanescent modes; in the context of guided wave propagation they go under the name of *surface waves* [27, §7].

The plate is subjected to free surface conditions

$$p_3(\xi_1, \pm\Theta^{-1}H, \xi_3, \tau) = 0, \qquad q_1(\xi_1, \pm\Theta^{-1}H, \xi_3, \tau) = 0. \qquad (3.12)$$

Using equations (2.1), (2.13), (2.14) into equation (2.17), the free boundary conditions (3.12) give

$$(1 - \delta^2)w' - \left[-(2 + \eta)\kappa^2 w + w''\right]' = 0 \qquad (3.13a)$$

and

$$w'' + \kappa^2 \eta w = 0, \qquad (3.13b)$$

where prime denotes differentiation with respect to the co-ordinate ξ_2.

(a) Extending Mindlin's mixed conditions to antiplane couple stress

As well known, in CE, Rayleigh–Lamb (RL) dispersion curves emerge from interference of fundamental waves, named *partial (or resonant) waves*, that are obtained imposing suitable boundary conditions [28–30]. For isotropic (transversely isotropic in general) materials, such conditions decouple into sagittal plane (plane-strain) and out-of-plane (antiplane) propagation [28].

In plane-strain propagation, the boundary conditions required to single out partial waves were first illustrated by [31] and are either the 'lubricated rigid wall' conditions

$$u_2 = 0, \qquad \sigma_{12} = 0, \qquad (3.14)$$

or the 'flexible micro-chain' conditions

$$u_1 = 0, \qquad \sigma_{22} = 0. \qquad (3.15)$$

Mindlin's conditions produce a pair of partial waves, named longitudinal (P) and SV partial waves, which travel across the plate thickness with an even or an odd integral number of half wavelengths (transverse resonance). Their name stems from the observation that the short-wave high-frequency (SWHF) limiting behaviour of P and SV partial waves asymptotes to longitudinal and shear bulk waves, respectively. Even P and even SV partial waves combine to give symmetric RL waves, while interference of odd P and odd SV waves gives antisymmetric (flexural) RL waves. Since no corresponding P partial wave exists in the region $V < 1$, symmetric and antisymmetric branches of the RL spectrum are guided, in the SWHF limit, by even and odd SV waves, respectively, the exception being the first branch which asymptotes to the Rayleigh wave speed.

When considering the motion out of the sagittal plane (antiplane motion), Mindlin's conditions are simply

$$\sigma_{23} = 0, \qquad (3.16)$$

and only one family of shear horizontal (SH or antiplane) partial wave exists in CE, with even and odd behaviour. As a consequence, no interference may occur and SH partial waves coincide with the corresponding antiplane guided RL waves. Furthermore, no Rayleigh wave speed is supported.
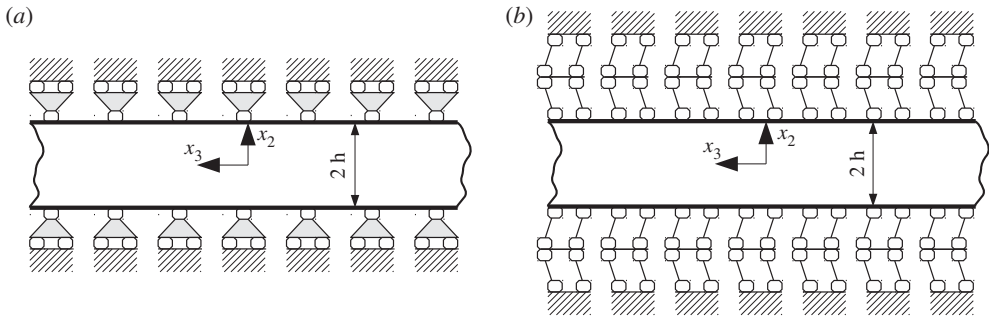
Figure 3. Sketch of the constraining conditions for the extended Mindlin's boundary conditions in the (x_2, x_3)-plane: (a) as in equation (3.17), (b) as in equation (3.18).

In the case of antiplane couple stress elasticity, the picture becomes more involved. We now prove that the generalization of Mindlin's boundary conditions (3.16) for antiplane motion in CS is either

$$w = m = 0, \tag{3.17}$$

or

$$w' = t = 0. \tag{3.18}$$

A graphical representation of such boundary conditions is given in figure 3.

(b) Wave reflection and mode conversion

The presence of a bulk evanescent wave gives rise to an interesting phenomenon of mode conversion between travelling waves and evanescent modes which has no parallel in CE. To see this, we consider a travelling wave impinging on either plate surface, say the top surface, at an incident angle α_1 with respect to ξ_2, in the presence of an evanescent mode travelling along ξ_1,

$$W(\xi_1, \xi_2) = B_1 \exp i \left[\delta(\sin \alpha_1 \xi_1 + \cos \alpha_1 \xi_2) \right] + B_2 \exp i \left[\delta(\sin \alpha_2 \xi_1 - \cos \alpha_2 \xi_2) \right]$$

$$+ B_4 \exp i \left[\delta \sin \alpha_1 \xi_1 \pm \iota \sqrt{1 + (\delta \sin \alpha_1)^2} \, \xi_2 \right]. \tag{3.19}$$

Here, B_1 is the amplitude of the impinging wave, B_2 the amplitude of the reflected wave forming an angle α_2 with ξ_2 and B_4 is the amplitude of the evanescent mode, see figure 4. In particular, the evanescent mode is so constructed that (a) it possesses the same wavenumber along ξ_1 as the impinging wave and (b) the wavevector has norm squared -1, i.e. it is indeed evanescent. Clearly, this evanescent mode is a surface wave. Such wave system satisfies the governing equation (3.3).

We observe that, if reflection at the surface of an half-plane is considered, then wave propagation occurs in $\xi_2 \leq 0$ and only the minus sign has to be taken in (3.19) to warrant depthwise decay (on account of the definition for the square root). In fact, if we reversed the direction of ξ_2, we would also need to change the sign of the ξ_2-component of the wave vector for the impinging wave and results would turn out the same. When, however, a plate is considered, both signs can be retained, i.e. two evanescent modes are triggered. This *non-uniqueness of the reflection* occurs also in CE for P-waves at grazing incidence [32, §3.1.4.5].

Imposing the first set of generalized Mindlin's boundary conditions, equation (3.17), we find that

$$\alpha_1 = \alpha_2 = \alpha, \tag{3.20}$$

and, as expected, no mode conversion occurs for

$$B_2 = -B_1, \qquad B_4 = 0.$$
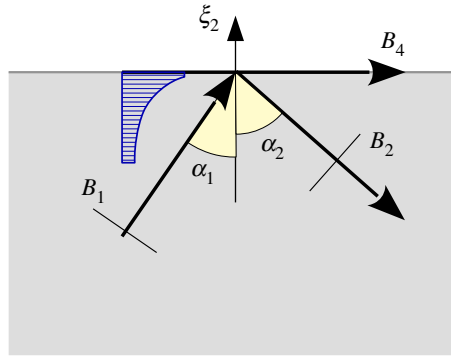
Figure 4. Travelling bulk shear plane wave B_1, impinging on a free surface with the angle α_1 to the surface normal, and generating a reflected travelling bulk shear wave B_2 plus a surface wave B_4. (Online version in colour.)

Indeed, this is a case of *total reflection* with π phase shift. This is at variance with respect to the behaviour of SH waves in CE, which reflect unaltered. In fact, this reflection scenario corresponds to that of P and SV waves hitting an in-plane constrained boundary, see [32, §3.1.1.2]. This result confirms that indeed (3.17) extends Mindlin's mixed boundary condition to CS elasticity.

Similarly, imposing the second set of Mindlin's boundary conditions, equation (3.18), we find again (3.20) and the wave reflects in its likeness (i.e. no phase shift) with no mode conversion

$$B_2 = B_1, \qquad B_4 = 0.$$

This result corresponds to mode conservation of SH waves in CE, see [32, §3.2.1].

Moving now to the free surface conditions (3.12), we get a system of equations depending on the sign in (3.19) for the evanescent wave. Accounting again for (3.20), this system gives the displacement reflection coefficients

$$\frac{B_2}{B_1} = - \exp(2i\theta_2), \qquad \frac{B_4}{B_1} = \Phi_4 \exp(-i\theta_4), \tag{3.21}$$

with

$$\theta_2 = \pm \arctan\left(\frac{b_2}{a_2}\right), \quad \Phi_4 = \frac{c_4}{|\Delta|}, \quad \tan\theta_4 = \cot\theta_2,$$

being

$$a_2 = \sqrt{2}\delta^3\sqrt{2 + \delta^2(1 - \cos 2\alpha_1)}\left[(\eta + 1)\cos(2\alpha_1) - \eta + 1\right]^2,$$

$$b_2 = 2\cos\alpha_1\left[\delta^2(\eta + 1)(1 - \cos 2\alpha_1) + 2\right]^2$$

and $\quad c_4 = 4\delta^2\cos\alpha_1\left[(\eta + 1)\cos(2\alpha_1) - \eta + 1\right]\left[\delta^2(\eta + 1)(1 - \cos 2\alpha_1) + 2\right].$

Here, $\Delta = a_2 - ib_2$ is the determinant of the system (3.13) and $|\Delta| = \sqrt{a_2^2 + b_2^2}$ its norm, that is always positive. Hence, we see that this is a case of *total reflection*, whereby the incident wave reflects with equal (in absolute term) amplitude and phase shift $2\theta_2 + \pi$. At the same time, an evanescent wave is triggered with reflection coefficient Φ_4 and phase shift $\theta_4 = \pi/2 - \theta_2$, see figure 5. A similar, but not equivalent, condition occurs in CE for the reflection of SV waves beyond the critical angle of incidence, with the P wave turning into a surface wave with complex amplitude [32, §3.1.4.5].

Reflection coefficients (3.21) are plotted in figure 5. We observe that the reflection coefficient B_4/B_1 is generally complex, which means that phase change occurs upon reflection into evanescent modes. The occurrence of complex reflection coefficients in CE is connected to the
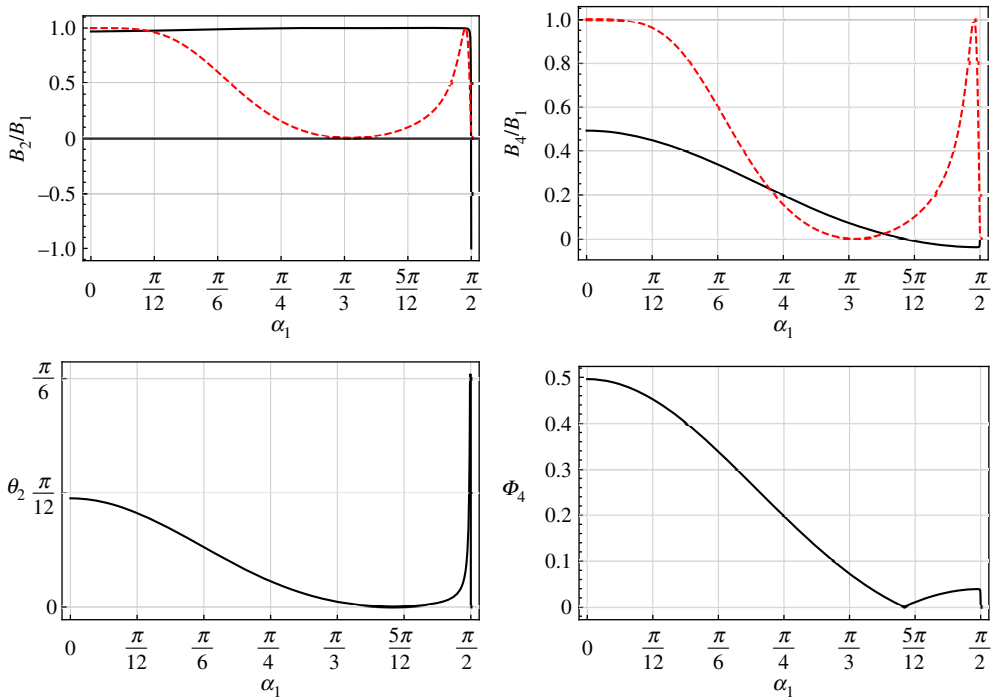
Figure 5. Real (solid, black) and imaginary part (dashed, red) of the reflection coefficients B_2/B_1 and B_4/B_1, phase angle θ_2 and amplitude ratio Φ_4 for an incident travelling wave, as a function of the angle of incidence α_1 ($\delta = 0.5$, $\eta = 0.1$). Total reflection, in the absence of mode conversion (i.e. $B_4 = 0$), is obtained at $\alpha_1 = 1.26452 \approx 5\pi/12$, according to equation (3.22). Here, minus has been chosen in (3.19), the case of plus being obtained by reversing the sign of the imaginary part of B_2 and B_4. (Online version in colour.)

incidence of SV waves taking place beyond the critical angle, which determines complex reflection angles for P waves [32, §3.1.2.2].

In light of (3.21), *total mode conversion* from travelling to evanescent modes is impossible, which result is expected in consideration of the fact that surface waves carry negligible energy compared to plane waves. Furthermore, total reflection generally triggers evanescent modes, with the notable exception of the critical incidence angle $\alpha_0 \geq \pi/4$

$$\cos(2\alpha_0) = 1 - \frac{2}{1+\eta}, \tag{3.22}$$

that exists provided that $\eta \geq 0$. For $\eta \ll 1$, we have the expansion

$$\alpha_0 = \tfrac{1}{2}\pi - \sqrt{\eta} + \frac{\eta^{3/2}}{3} + \cdots \tag{3.23}$$

that is shown in figure 6 alongside the exact curve. The plot is remarkable for it shows that, at $\eta = 0$, we have $\alpha_0 = \pi/2$, that is grazing incidence. As it will presently appear, the existence of Rayleigh waves is connected to the appearance of evanescent modes precisely at grazing incidence and, in fact, the situation $\eta = 0$ does not support antiplane Rayleigh waves.

Approaching grazing incidence, i.e. as the angle of emergence $\epsilon = \tfrac{1}{2}\pi - \alpha$ tends to zero, the $O(1)$ term in the solution vanishes and we have

$$W(\xi_1, \xi_2) = \epsilon W_1(\xi_1, \xi_2) + \epsilon^2 W_2(\xi_1, \xi_2) + \cdots. \tag{3.24}$$

Thus, the leading order term in the expansion of the displacement is

$$W_1(\xi_1, \xi_2) = \mp B_1' e^{i\delta\xi_1} + B_2'\xi_2 e^{i\delta\xi_1} \pm B_4' e^{i\delta\xi_1 + \sqrt{1+\delta^2}\xi_2}, \tag{3.25}$$
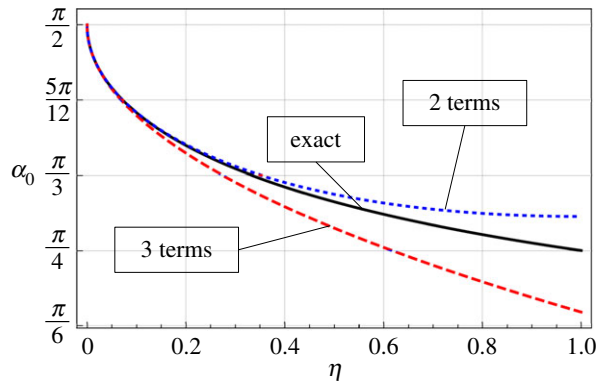
Figure 6. Critical angle for total reflection in the absence of mode conversion as a function of η (black, solid), alongside the two- (red, dashed) and three-term (blue, dotted) expansions. (Online version in colour.)

with the coefficients

$$B'_1 = 2\mathrm{i}\,\frac{\zeta_{11}^2(\delta)}{\eta^2\delta^3\sqrt{1+\delta^2}}B_1, \quad B'_2 = \frac{\eta^2\delta^4\sqrt{1+\delta^2}}{\zeta_{11}^2(\delta)}B'_1, \quad B'_4 = \frac{\eta\delta^2}{\zeta_{11}(\delta)}B'_1, \tag{3.26}$$

where we have let

$$\zeta_{11}(\kappa) = (1+\eta)\kappa^2 + 1, \qquad \zeta_{12}(\kappa,\delta) = (1+\eta)\kappa^2 - \delta^2.$$

Hence, we have an 'incident' plane travelling wave, B'_1, that generates a 'reflected' travelling wave, B'_2, whose amplitude is proportional to ξ_2 and thereby it is sometimes denoted SHy, plus a surface wave B'_4. All such waves move along ξ_1 with speed c_{SH}. Together, incident and reflected waves represent the most general form of bulk shear plane waves (see also [33]), while the surface wave is a bulk evanescent mode, for its wavevector is complex-valued with norm -1, and it exists only inasmuch as $\eta \neq 0$.

At normal incidence, $\alpha = 0$, we get

$$\theta_2 = \pm \arctan \delta^{-3}, \quad \varPhi_4 = \frac{2\delta^2}{\sqrt{1+\delta^6}}, \quad \theta_4 = \pm \arctan \delta^3, \tag{3.27}$$

depending on the sign in (3.19) and irrespective of η. This result differs substantially from the corresponding result in CE, where reflection at normal incidence occurs in the absence of mode conversion [32, §3.1.4.1]. Indeed, in CS elasticity, we always have the appearance of an evanescent mode, regardless of η.

(c) Reflection of evanescent modes

Equation (3.19) does not exhaust all possible scenarios of wave reflection at a free surface. Indeed, with an approach that has no counterpart in CE, we may consider reflection of evanescent modes. To see this, we consider a system of waves in the form

$$W(\xi_1, \xi_2) = B_1 \exp\left(-\sin\alpha_1\xi_1 - \cos\alpha_1\xi_2\right) + B_2 \exp\left(-\sin\alpha_2\xi_1 + \cos\alpha_2\xi_2\right)$$

$$+ B_4 \exp\mathrm{i}\left(\mathrm{i}\sin\alpha_1\xi_1 + \sqrt{\sin^2\alpha_1 + \delta^2}\,\xi_2\right), \tag{3.28}$$

where the first two contributions represent evanescent bulk plane standing waves and the last is an evanescent bulk wave (with wavevector norm δ) that travels along ξ_2 and decays along ξ_1, i.e. it is a surface wave, see figure 7. Strictly speaking, B_1 is not impinging on the boundary, for it is not travelling, yet its presence in the bulk is tied with the appearance, due to the boundary,
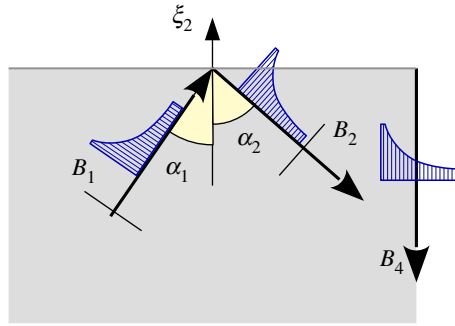
Figure 7. Evanescent bulk standing wave B_1, acting on a free surface with the angle α_1 to the surface normal and generating a 'reflected' standing bulk wave B_2 together with a Rayleigh-like wave B_4 travelling in the direction normal to the surface. (Online version in colour.)

of the other pair of waves. This wave system satisfies the governing equation (3.3) and, upon assuming (3.20), it is 'reflected' with no mode conversion, when subjected to either of the extended Mindlin's conditions (3.18) or (3.17). Consequently, these mixed boundary conditions work for evanescent modes just as well as for travelling modes.

On a free surface, we get the displacement reflection coefficients

$$\frac{B_2}{B_1} = \exp(2\mathrm{i}\theta_2'), \qquad \frac{B_4}{B_1} = \Phi_4' \exp(-\mathrm{i}\theta_4'), \tag{3.29}$$

with

$$\theta_2 = \arctan(b_2'/a_2'), \quad \Phi_4 = \frac{c_4'}{\sqrt{a_2'^2 + b_2'^2}}, \quad \theta_4' = -\theta_2',$$

being

$$a_2' = 4\cos\alpha_1 \left[2\delta^2 + \eta + 1 - (1+\eta)\cos(2\alpha_1)\right]^2,$$

$$b_2' = 2\sqrt{2}\sqrt{1 + 2\delta^2 - \cos(2\alpha_1)}\left[(\eta+1)\cos(2\alpha_1) - \eta + 1\right]^2$$

and

$$c_4' = 8\cos\alpha_1\left[(\eta+1)\cos(2\alpha_1) - \eta + 1\right]\left[2\delta^2 + \eta + 1 - (\eta+1)\cos(2\alpha_1)\right].$$

Reflection coefficients (3.29) are plotted in figure 8. They equal the corresponding coefficients for travelling waves (3.21) when $\delta = 1$, for then the Rayleigh function is centrally symmetric. The critical angle that triggers no surface mode B_4 is again given by equation (3.22). The reflection coefficients at normal incidence, $\alpha = 0$, are given by

$$\theta_2' = -\theta_4' = \arctan\delta^{-3}, \qquad \Phi_4' = \frac{2\delta^2}{\sqrt{1+\delta^6}}. \tag{3.30}$$

In the limit of grazing incidence, the zero-order solution disappears and we consider an expansion in the angle of emergence $\epsilon = \pi/2 - \alpha_1$ as in (3.24). The leading order solution consists of two standing waves plus a Rayleigh-like wave, that travels *away from* the surface at a speed smaller than that of shear bulk waves,

$$W_1(\xi_1, \xi_2) = B_1'' e^{-\xi_1} - B_4'' e^{-\xi_1 + \mathrm{i}\sqrt{\delta^2+1}\xi_2} + B_2'' \xi_2 e^{-\xi_1} + O(\epsilon^2), \tag{3.31}$$

having let

$$B_1'' = 2\mathrm{i}\frac{(\delta^2 + \eta + 1)^2}{\eta^2\sqrt{1+\delta^2}}B_1, \quad B_4'' = \frac{\eta}{\delta^2 + \eta + 1}B_1'', \quad B_2'' = \mathrm{i}\frac{\eta^2\sqrt{1+\delta^2}}{(\delta^2+\eta+1)^2}B_1''. \tag{3.32}$$
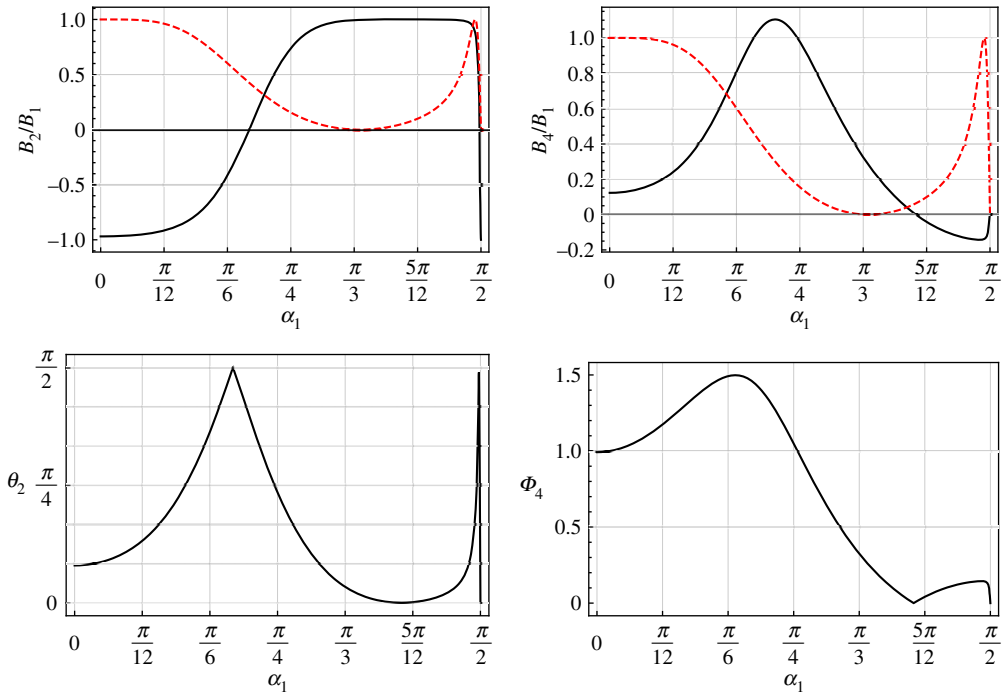
Figure 8. Real (solid, black) and imaginary part (dashed, red) of the reflection coefficients B_2/B_1 and B_4/B_1, phase angle θ_2 and amplitude ratio Φ_4 for *evanescent modes*, as a function of the angle of incidence α_1 ($\delta = 0.5$, $\eta = 0.1$). Total reflection, in the absence of mode conversion (i.e. $B_4 = 0$), is obtained at $\alpha_1 = 1.26452 \approx 5\pi/12$, according to equation (3.22). (Online version in colour.)

(d) Classification of the Rayleigh zeros

We consider the general decaying solution for an half-plane $\xi_2 \leq 0$ [32, §3.1.4.7]

$$w(\xi_2) = e_1 \exp(\lambda_1 \xi_2) + e_2 \exp(\lambda_2 \xi_2), \tag{3.33}$$

provided that branch cuts in the square root are taken as to give positive real part on the real axis, see [6]. Plugging this form into the boundary conditions (3.13) and demanding for non-trivial solutions to exist, yields the Rayleigh function

$$R(\kappa, \delta) = \zeta_{11}^2 \lambda_1 - \zeta_{12}^2 \lambda_2. \tag{3.34}$$

Zeros and branch-points for the Rayleigh function are presented in figure 9. The Rayleigh wavenumber κ_R is obtained looking for the real root of

$$R(\kappa, \delta) = 0, \tag{3.35}$$

and the corresponding eigenform is given by

$$W(\xi_1, \xi_2) = e^{i\kappa_R \xi_1} \left[e^{\sqrt{\kappa_R^2 - \delta^2} \xi_2} - \frac{\zeta_{12}(\kappa_R, \delta)}{\zeta_{11}(\kappa_R)} e^{\sqrt{\kappa_R^2 + 1} \xi_2} \right]. \tag{3.36}$$

The special case $\eta = 0$ is interesting for we have

$$R(\kappa, \delta) = -\lambda_1 \lambda_2 (\lambda_1^3 - \lambda_2^3)$$

which possesses the obvious order 1/2 roots $\kappa = \pm \delta$ and $\kappa = \pm i$, respectively corresponding to bulk SH and bulk evanescent waves, i.e. as anticipated, for $\eta = 0$, Rayleigh waves collapse into bulk waves.
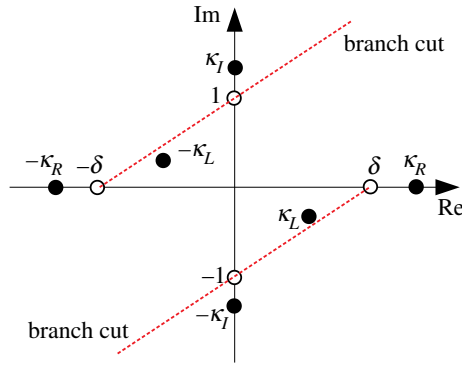
14

royalsocietypublishing.org/journal/rspa Proc. R. Soc. A **476**: 20190822

Figure 9. Branch-points (circles), zeros (dots) and branch cuts (dashed line) for the Rayleigh function $R(\kappa, \delta)$, given by equation (3.34). (Online version in colour.)

The Rayleigh wavenumber κ_R may be expressed in terms of the distance from the bulk shear wavenumber δ,

$$\kappa_R = \delta \left(1 + \kappa_{1R}^2\right), \quad \text{with } \kappa_{1R}^2 = \frac{\delta^6(1 + \delta^2)}{2\zeta_{11}^4(\delta)} \eta^4 \ll 1, \tag{3.37}$$

from which we see that $\kappa_R > \delta$ and therefore $c_R < c_{SH}$ inasmuch as $\eta \neq 0$, i.e. the Rayleigh wave speed is lower than the bulk wave speed. Given that $|\eta| < 1$, we see that equation (3.37) is extremely accurate, in light of the fact that $\kappa_{1R}^2 = O(\eta^4)$. Rayleigh waves come in pairs and decay exponentially depth-wise with attenuation indices that may be expanded in powers of κ_{1R}

$$\lambda_1 = \sqrt{2}\delta\kappa_{1R} + O(\kappa_{1R}^3), \qquad \lambda_2 = \sqrt{1 + \delta^2} + O(\kappa_{1R}^2),$$

whence (3.36) lends (we take $e_1 = B_1'$)

$$W_R(\xi_1, \xi_2) = B_1' e^{i\delta\xi_1} - B_4' e^{i\delta\xi_1 + \sqrt{1+\delta^2}\xi_2} + B_2' \xi_2 e^{i\delta\xi_1} + O(\kappa_{1R}^2). \tag{3.38}$$

We observe that equation (3.38) perfectly matches the leading order term in the expansion of the displacement (3.25), when approaching grazing incidence. Indeed, we can interpret the grazing incident solution as the expansion of the Rayleigh solution in the small parameter κ_{1R}, expressing the distance of the Rayleigh wavenumber from the bulk shear-wave wavenumber. However, relating the two expansions is not straightforward, for the leading order term solution at grazing incidence, W_1, matches the leading and first correction terms of the Rayleigh expansion W_R. Indeed, $B_2' = \sqrt{2}\kappa_{1R}B_1'$ brings a small term correction in (3.38). Still, it is tantalizing to interpret Rayleigh waves as being originated from the reflection of bulk shear waves impinging on the free surface at 'almost' grazing incidence, the distance from perfect grazing being related to their slowness with respect to bulk shear waves.

Equation (3.35) admits the pair of purely imaginary zeros $\pm\kappa_I$, that are located close to the purely imaginary branch points $\pm i$, see figure 9. Writing κ_I in terms of the distance from ι, we find

$$\kappa_I = i\left(1 + \kappa_{1I}^2\right), \quad \text{with } \kappa_{1I}^2 = \frac{1 + \delta^2}{2(1 + \delta^2 + \eta^2)^4} \eta^4 \ll 1.$$

Looking at the attenuation indices, it is

$$\lambda_1 = i\sqrt{1 + \delta^2} + O(\kappa_{1I}^2), \quad \text{and} \quad \lambda_2 = i\sqrt{2}\kappa_{1I} + O(\kappa_{1I}^3),$$

and we have the expansion

$$W_I(\xi_1, \xi_2) = B_1'' e^{-\xi_1} - B_4'' e^{-\xi_1 + i\sqrt{\delta^2+1}\xi_2} + B_2'' \xi_2 e^{-\xi_1} + O(\kappa_{1I}^2), \tag{3.39}$$
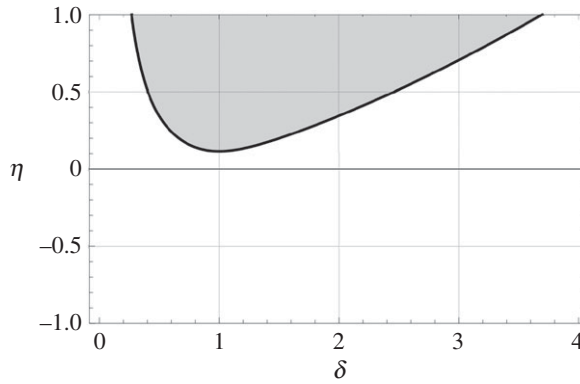
Figure 10. Domain (δ, η) for the complex root κ_L to sit in the physical Riemann sheet: when moving outside the shaded area, κ_L slips through the branch cut out of the physical sheet. The domain shape is independent of ℓ_0 and existence of the root is possible only inasmuch as $\eta > \eta_L$.

with

$$B_1'' = -\frac{\delta^2 + \eta + 1}{\eta} e_1, \quad B_2'' = i\sqrt{2}\kappa_{1I}B_1'', \quad B_4'' = \sqrt[4]{\frac{2\kappa_{1L}^2}{1 + \delta^2}}B_1''. \tag{3.40}$$

Again, the wave system (3.39) with the coefficients (3.40) matches the expansion of the evanescent mode wave system (3.31), (3.32) when approaching grazing incidence. We conclude that the purely imaginary zero of the Rayleigh equation expresses a perturbation of the grazing incident condition for bulk evanescent modes, the distance from it (along the imaginary axis) expressing how stronger the decay rate is with respect to the bulk mode. We note that none of the three terms in this system is a proper leaky wave, i.e. according to [34] 'an inhomogeneous wave that propagates along the surface with a phase velocity larger than the shear wave but smaller than the pressure wave'. In fact, the B_4'' term looks more like a Rayleigh wave moving *away from*, rather than *along*, the free surface with speed $c < c_{SH}$. This is precisely the wave found in [6] radiating from the tip of a semi-infinite rectilinear crack. Thus, the claim put forward in [34], according to which any complex solution of the Rayleigh function is a leaky wave, does not hold in CS elasticity.

Equation (3.34) possesses the extra pair of complex roots $\kappa = \pm\kappa_L$, provided that parameters (δ, η) lay in the domain of figure 10. This domain of existence is mapped onto the (Ω, η) plane, for different values of ℓ_0, in figure 11. The root κ_L sits close to the branch cut and for it we choose $\Im(\kappa_L)\Re(\kappa_L) < 0$ (see figure 9). Its precise location may be found explicitly only for $\delta = 1$, making the observation that in such special situation κ_L lies on the fourth quadrant bisector

$$\kappa_L = \gamma_L \exp(-i\pi/4), \qquad \gamma_L = \sqrt[4]{\frac{-1 - 3\eta + 2\sqrt{1 + 2\eta + 2\eta^2}}{(1 + \eta)^2(3 - \eta)}}.$$

Using (3.6), we see that $\delta = 1$ corresponds to $\Omega = \ell_0^{-1}$, provided that $\ell_0 \neq 0$. Under the connection $\nu = -\eta$, γ_L becomes proportional to Konenkov's well known constant $\gamma_e = [(1 - \nu) (3\nu - 1 + 2\sqrt{1 - 2\nu + 2\nu^2})]^{1/4}$ arising in edge-wave propagation in a plate [35]. The root is admissible inasmuch as it rests inside the branch cut, i.e. $|\kappa_L| < \sqrt{2}/2$ that demands $\eta > \eta_L$ where $\eta_L = \sqrt{2(5 - \sqrt{5})} - \sqrt{5} \approx 0.1151$. Interestingly, η_L is also the minimum value of η that is capable of supporting the root κ_L in the physical sheet in general, that is for any ℓ_0, see figure 11. Indeed, γ_L is a decreasing function of η, whose minimum 0.492883 is attained for $\eta = 1$.
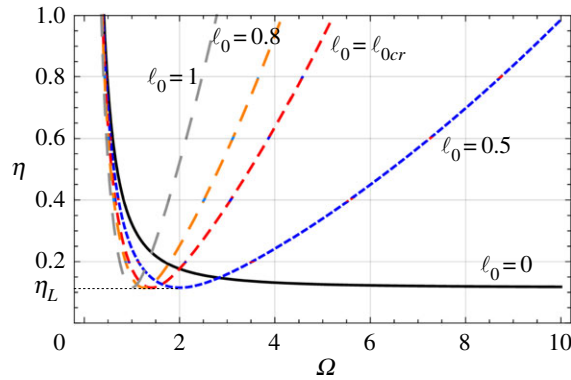
Figure 11. The way the parameter ℓ_0 affects the shape of the domain of existence of κ_L can be appreciated only in the plane (Ω, η). (Online version in colour.)

Plugging $\kappa = \pm\kappa_L$ into the eigenmode (3.36), we get

$$W(\xi_1, \xi_2) = e^{\pm \frac{1+i}{\sqrt{2}}\gamma_L \xi_1} \left(e^{\sqrt{-1-i\gamma_L^2}\xi_2} + \frac{i - \gamma_L^2(\eta + 1)}{i + \gamma_L^2(\eta + 1)} e^{\sqrt{1-i\gamma_L^2}\xi_2} \right),$$

and the first (second) exponential term inside the parenthesis has negative (positive) real part argument. Consequently, either root is associated with a pair of waves that propagate and explode (decay in the case of $-\kappa_L$) along the free surface, with a longitudinal speed $c_L = \sqrt{2}\delta c_{SH}/\gamma_L$ greater than that of bulk shear waves c_{SH}. One wave *decays* moving away from the surface, the other explodes. Consequently, these are not leaky waves either, at least according to the classical definition. Furthermore, it is unclear what bulk wave such roots couple with, for they are perturbations of none. We also point out that, at variance with [34], for a half-plane we are not free to choose the sign in front of square roots $\lambda_{1,2}$, that is univocally determined by the choice of the branch cuts. Such choice is determined by Sommerfeld's condition and by the boundedness requirement at infinity, as detailed in [36] and in [6].

On account of these results, we suggest the classification work-flow of figure 12 for the zeros of the Rayleigh function. This classification is not complete, for it only covers the possibilities explored in this paper.

(e) Antiplane partial waves

We now apply the extended Mindlin's conditions for CS, equations (3.17) and (3.18), to the case of guided propagation in a plate. Demanding that the even (odd) part of the boundary conditions vanishes, produces odd

$$\cosh\left(\Theta^{-1}\lambda_1 H\right)\cosh\left(\Theta^{-1}\lambda_2 H\right) = 0, \tag{3.41}$$

and even partial waves

$$\sinh\left(\Theta^{-1}\lambda_1 H\right)\sinh\left(\Theta^{-1}\lambda_2 H\right) = 0. \tag{3.42}$$

Only one family of antiplane *travelling* partial waves exist, namely those associated with λ_1 (figure 13),

$$\kappa^2 - \delta^2 = -\left(n\frac{\Theta\pi}{2H}\right)^2, \quad n = 0, 1, 2, \ldots, \tag{3.43}$$

the first of which, attained for $n = 0$, corresponds to SH bulk waves. For this reason, and in analogy with RL partial waves in CE, we denote such waves as SH partial waves. It is important to observe that, in the SWHF limit, equation (3.43) gives $\kappa \to \delta$ from *below* and the bulk SH wave speed is approached from above, i.e. partial waves are supersonic. According to the parity of n,
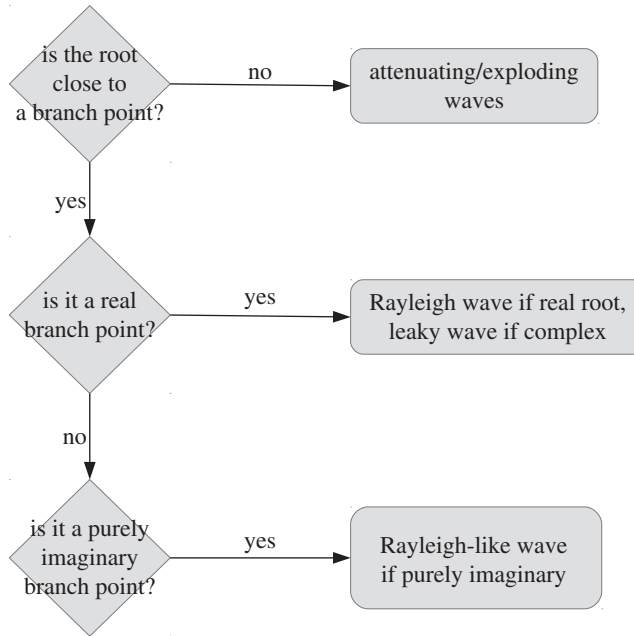
Figure 12. Classification work-flow for the Rayleigh zeros.

we distinguish even and odd partial waves, the former set being composed by the level curves $\sinh(\Theta^{-1}\lambda_1 H) = 0$ and the latter by the solution curves $\cosh(\Theta^{-1}\lambda_1 H) = 0$. Using equation (3.5), the group velocity of SH partial waves may be written as

$$V_g = \frac{2\delta_{cr}\delta - ((n\pi)/2H)^2}{2K},$$
(3.44)

that is always positive for the first branch in general and for all branches when a thick plate is considered, i.e. as $H \to +\infty$. Indeed, in the latter case, partial waves collapse into SH body waves.

In light of equation (3.10), we see that partial waves associated with λ_2 are evanescent, for they are connected with a purely imaginary wavenumber $\kappa = i\bar{\kappa}$, $\bar{\kappa} > 0$. However, as we have just shown when discussing wave reflection, they are equally important, because they may combine with travelling waves at the boundaries. Besides, such waves originate localized effects when semi-infinite or finite domains are dealt with, e.g. see [35]. They are given by

$$\bar{\kappa}^2 = 1 + \left(n\frac{\Theta\pi}{2H}\right)^2, \quad n = 0, 1, 2, \ldots,$$
(3.45)

and the case $n = 0$ corresponds to bulk evanescent waves. Interestingly, evanescent modes possess positive (negative) group velocity, inasmuch as $\ell_0 \lessgtr \ell_{0cr}$. Besides, in consideration of the monotonic behaviour of Θ, see figure 2, we see that evanescent modes exists in the bounded range $\bar{\kappa}_m < \bar{\kappa} < \bar{\kappa}_M$, where

$$\bar{\kappa}_m = \min\left(\bar{\kappa}^{(LWLF)}, \bar{\kappa}^{(SWHF)}\right), \qquad \bar{\kappa}_M = \max\left(\bar{\kappa}^{(LWLF)}, \bar{\kappa}^{(LWLF)}\right),$$

being

$$\bar{\kappa}^{(LWLF)} = 1 + \tfrac{1}{2}\left(n\frac{\pi}{2H}\right)^2, \qquad \bar{\kappa}^{(SWHF)} = 1 + \left(n\frac{\ell_0\pi}{2H}\right)^2.$$

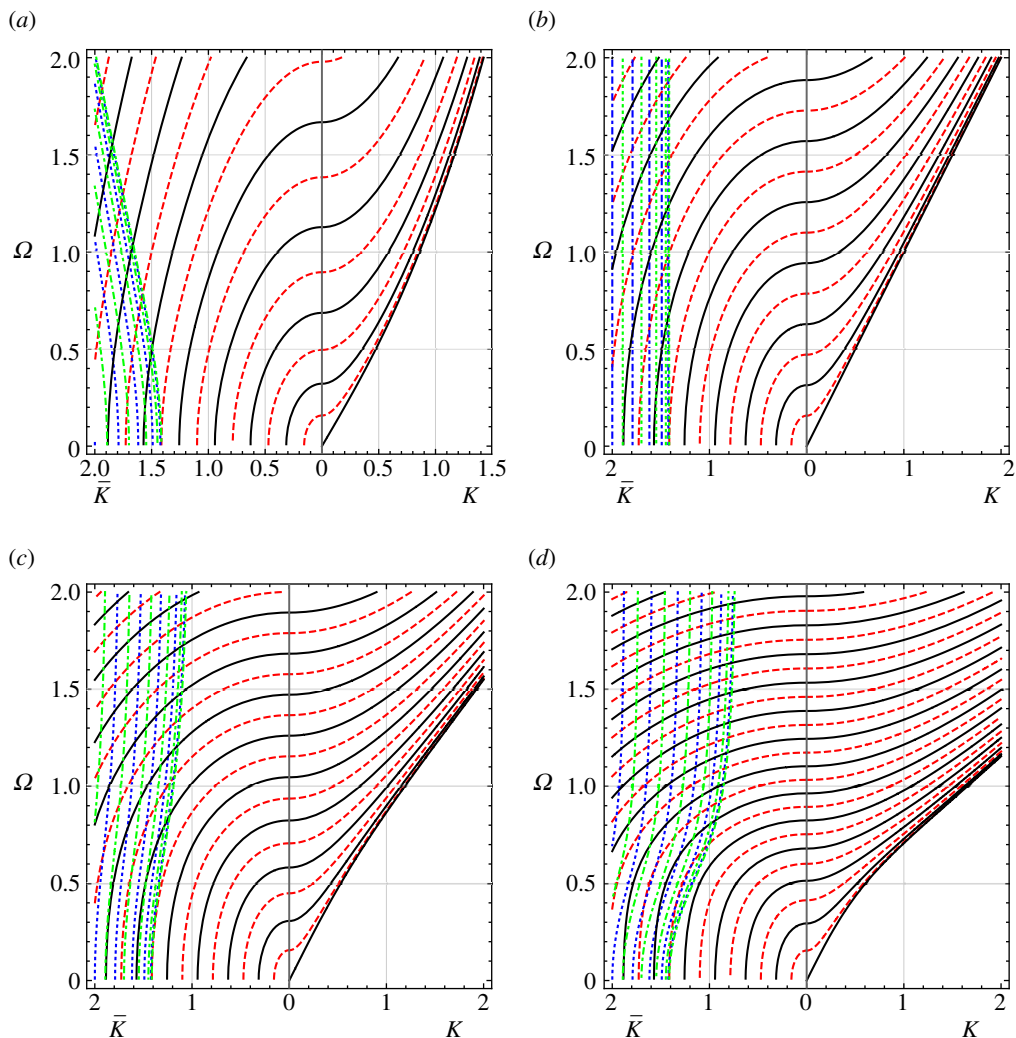In the SWHF regime, they asymptote to the wavenumber $\bar{\kappa}^{(SWHF)}$.

Figure 13. Even (solid, black) and odd (dashed, red) antiplane travelling partial waves frequency spectrum ($\eta = 0.1$, $H = 10$) superposed onto evanescent even (dotted, blue) and odd (dashed-dotted, green) partial waves. (*a*)$\ell_0 = 0.1$, (*b*) $\ell_0 = \ell_{0cr}$, (*c*) $\ell_0 = 1$, and (*d*) $\ell_0 = \sqrt{2}$. (Online version in colour.)

4. Antiplane Rayleigh–Lamb waves

We are now in a position to discuss antiplane RL waves in CS isotropic materials. They will emerge from combination of travelling and evanescent partial waves through the boundary conditions. To a certain extent, the process is similar to what occurs in plane-stain CE, where two families of travelling waves interact.

(a) Symmetric waves

We now consider symmetric waves, i.e. waves whose profile is an even function of ξ_2. Then, we enforce that the odd part of p_3 and the even part of q_1 vanish at $\xi_2 = H/\Theta$, whence we get a linear system in the even vector $\boldsymbol{\psi}_e = [e_1, e_2]$

$$\mathbf{S}\boldsymbol{\psi}_e = \boldsymbol{o},$$
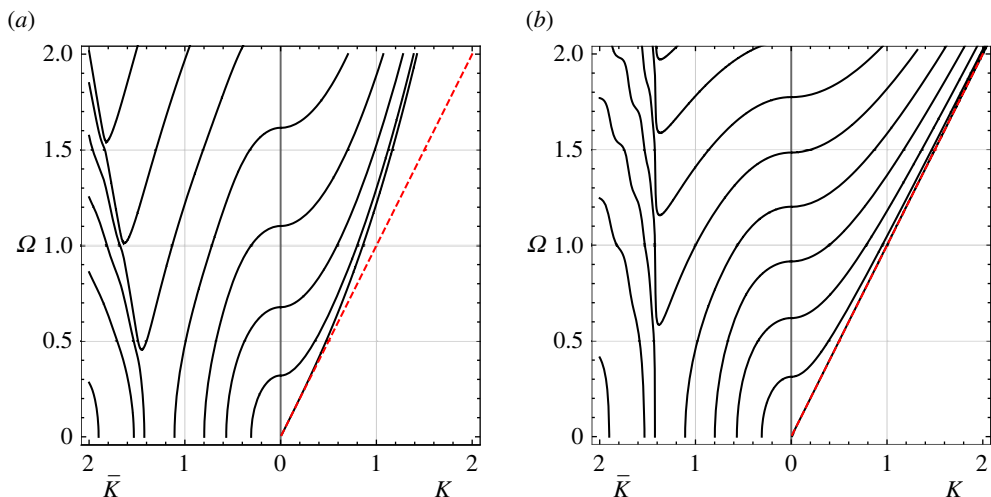
Figure 14. Frequency spectrum for symmetric antiplane Rayleigh–Lamb waves (solid, black) superposed onto the LWLF approximation (4.2) (dashed, red) ($\eta = 0.1, H = 10$). (a)$\ell_0 = 0.1$ and (b) $\ell_0 = \ell_{0cr}$. (Online version in colour.)

where

$$\mathbf{S} = \begin{bmatrix} \zeta_{11}\lambda_1 \sinh\left(\Theta^{-1}\lambda_1 H\right) & \zeta_{12}\lambda_2 \sinh\left(\Theta^{-1}\lambda_2 H\right) \\ \zeta_{12} \cosh\left(\Theta^{-1}\lambda_1 H\right) & \zeta_{11} \cosh\left(\Theta^{-1}\lambda_2 H\right) \end{bmatrix}.$$

The frequency equation $d_s(\kappa, \Omega) = 0$, where

$$d_s(\kappa, \Omega) = \zeta_{11}^2 \lambda_1 \sinh\left(\Theta^{-1}\lambda_1 H\right)\cosh\left(\Theta^{-1}\lambda_2 H\right) - \zeta_{12}^2 \lambda_2 \sinh\left(\Theta^{-1}\lambda_2 H\right)\cosh\left(\Theta^{-1}\lambda_1 H\right), \quad (4.1)$$

is plotted in figure 14. The SWHF behaviour of the real spectrum is guided from above by even partial waves, see figure 15. In particular, the first branch of the plot rests little below the first even partial wave (that is the bulk shear wave), i.e. for a given Ω we have $\kappa > \delta$. Consequently, since λ_1 and λ_2 are real numbers in the region $\kappa > \delta$, we see that equation (4.1) tends to the Rayleigh equation (3.35) and therefore $\kappa \to \kappa_R$ from above. Thus, as it occurs in CE, we obtain the well-known result by which, in the SWHF limit, the lowest travelling mode (that is even) propagates in a plate as a Rayleigh wave. Obviously, the same behaviour is retrieved letting $H \to \infty$. All other branches are located in the region $\kappa < \delta$, wherein $\lambda_1 = i\bar{\lambda}_1$ is purely imaginary. Given that such branches are located in between two adjacent partial modes, like those they asymptote to the bulk shear wavenumber. This different limiting behaviour of the first branch than higher symmetric modes, is difficult to capture numerically. For example, in [18], in the context of sagittal propagation, it is claimed that 'as the frequency increases, all modes converge to the Rayleigh wave propagation speed'.

Upon considering equation (3.43) and the limit behaviour (3.8), the asymptotic model [37] for symmetric antiplane waves in the long-wave low-frequency (LWLF) range is, to leading order in Ω,

$$K^2 - \Omega^2 = 0, \quad (4.2)$$

regardless of η, H and ℓ_0. In fact, this model is exact for the entire first branch, that is non-dispersive, when $\ell_0 = \ell_{0cr}$, see figure 14b. This non-dispersive character of the lowest RL mode also occurs in CE [15, §8.1.1]. The corresponding eigenform, to leading order, is simply
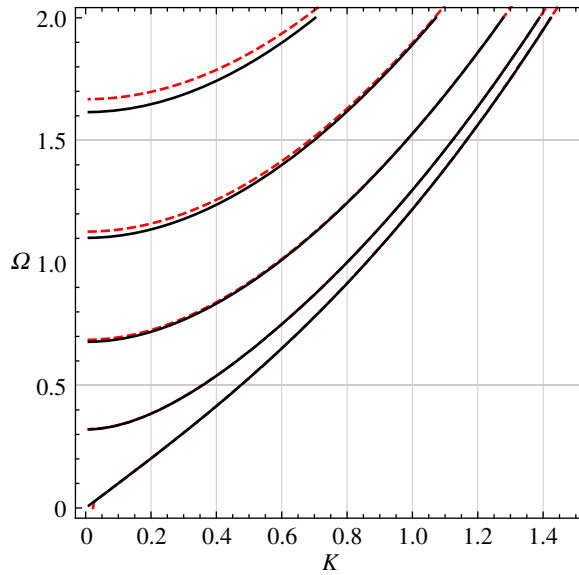
$$w(\xi_2) = e_2 \cosh \xi_2.$$

Figure 15. Symmetric antiplane RL waves (solid, black) and even SH partial waves (dashed, red) frequency spectrum ($\eta = 0.1$, $\ell_0 = 0.1$, $H = 10$). In the SWHF limit, all branches but the first asymptote to the bulk SH wavenumber $\kappa = \delta$; instead, the first branch approaches the Rayleigh wavenumber $\kappa_R > \delta$ from above (i.e. from lower speed). (Online version in colour.)

Equation (4.2) provides the leading order differential model for the lowest antiplane vibration mode for a plate made of CS elastic material

$$\frac{\partial^2 W}{\partial x_1^2} - \frac{1}{c_s^2}\frac{\partial^2 W}{\partial t^2} = 0, \tag{4.3}$$

corresponding to travelling waves moving at speed c_s, that is the shear wave speed in CE. This model may be refined in the thin plate limit $H \ll 1$, for then equation (4.1) yields, to leading order in H,

$$d_{st}(\kappa, \Omega) = \zeta_{11}^2 \bar{\lambda}_1^2 + \zeta_{12}^2 \lambda_2^2 = (1 + \delta^2)\left[-(1 - \eta^2)\kappa^4 + (\delta^2 - 1)\kappa^2 + \delta^2\right], \tag{4.4}$$

which corresponds to the differential model in the LWLF regime

$$-\tfrac{1}{2}(1 - \eta^2)K^4 - K^2 + \tfrac{1}{2}\Omega^2 K^2 + \Omega^2 = 0. \tag{4.5}$$

When moving back to operators, equation (4.5) gives the same governing equation as for Rayleigh flexural beam-columns

$$-\tfrac{1}{2}\ell^2(1 - \eta^2)\frac{\partial^4 W}{\partial x_1^4} + \frac{\partial^2 W}{\partial x_1^2} + \tfrac{1}{2}T^2\frac{\partial^2 W}{\partial x_1^2 \partial t^2} - \frac{1}{c_s^2}\frac{\partial^2 W}{\partial t^2} = 0, \tag{4.6}$$

where the second term accounts for a tensile loading and the third term provides rotational inertia. This differential model governs antiplane symmetric vibrations of thin beam-plates made of CS material, as in figure 16. Remarkably, this model is independent on ℓ_d and therefore on rotational inertia. We point out that this PDE corresponds to eqn (19) of [38], that provides the simplest description for waves propagating in microstructured continua whose internal lengthscale is much smaller than the propagating wavelength. As illustrated in [38], 'The special feature of this approximation is that it can be used over the whole range of wavenumbers, since it does not represent a short-wave or long-wave approximation. The underlying assumption is that the influence of the microstructure is small'. Also, simplified versions of (4.6) are not accurate, as shown in figure 14a.
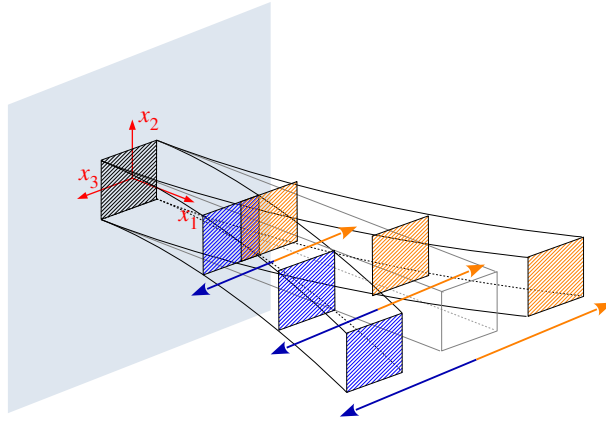
Figure 16. Antiplane symmetric (about the mid-plane $x_2 = 0$) vibrations of a beam-plate made of CS elastic material (for the sake of clarity, in this picture, an element of finite thickness along x_3 is shown). Since antiplane vibrations are dealt with, shaded cross sections move parallel to the (x_2, x_3) plane. (Online version in colour.)

It is worth marking the difference with CE, where thin-plate transversal vibrations are simply described by the wave equation (4.3). This limiting case may be easily retrieved from equation (4.6), by simply taking $\ell = 0$ (and consequently $T = 0$). Besides, we observe that, in the case of the modified couple stress theory, that occurs for $\eta = 1$, the first term of (4.6) drops out and the differential model reduces to that of a vibrating string with rotational inertia. In this case, we have a problem accommodating the right number of boundary conditions. Indeed, this outcome is expected, for the case $1 - \eta \ll 1$ leads to a singularly perturbed model and to the appearance of a boundary layer.

(b) Antisymmetric waves

For antisymmetric RL waves, we have the linear system in the odd vector $\boldsymbol{\psi}_o = [o_1, o_2]$

$$\mathbf{A}\boldsymbol{\psi}_o = \boldsymbol{o},$$

where

$$\mathbf{A} = \begin{bmatrix} \zeta_{11} \cosh\left(\Theta^{-1}\lambda_1 H\right) & \zeta_{12} \cosh\left(\Theta^{-1}\lambda_2 H\right) \\ \zeta_{12}\lambda_1^{-1} \sinh\left(\Theta^{-1}\lambda_1 H\right) & \zeta_{11}\lambda_2^{-1} \sinh\left(\Theta^{-1}\lambda_2 H\right) \end{bmatrix}.$$

The dispersion relation $d_o(\kappa, \Omega) = 0$, with

$$d_o(\kappa, \Omega) = \zeta_{11}^2 \lambda_2^{-1} \cosh(\Theta^{-1}\lambda_1 H) \sinh(\Theta^{-1}\lambda_2 H) - \zeta_{12}^2 \lambda_1^{-1} \sinh(\Theta^{-1}\lambda_1 H) \cosh(\Theta^{-1}\lambda_2 H), \quad (4.7)$$

is plotted in figure 17. The frequency spectrum branches are guided by odd partial waves (3.41), see figure 18. The cut-off frequencies Ω_n^* are obtained from solving the transcendental equation $d_o(0, \Omega) = 0$, that gives

$$\delta^3 \tan\left(\Theta^{-1}H\delta\right) = \tanh\left(\Theta^{-1}H\right). \quad (4.8)$$

This equation, besides Ω, depends on the parameters ℓ_0 and H. It may be approximated, for $H \ll \Theta$, to the simple form for the cut-off equation

$$\delta = \delta^* = 1, \quad \Rightarrow \Omega^* = \ell_0^{-1}. \quad (4.9)$$

We observe that this is exactly the situation discussed in connection with the root κ_I of the Rayleigh function. Conversely, for $H \gg \Theta$, a very good approximation is

$$\delta^3 \tan\left(\Theta^{-1}H\delta\right) = 1. \quad (4.10)$$
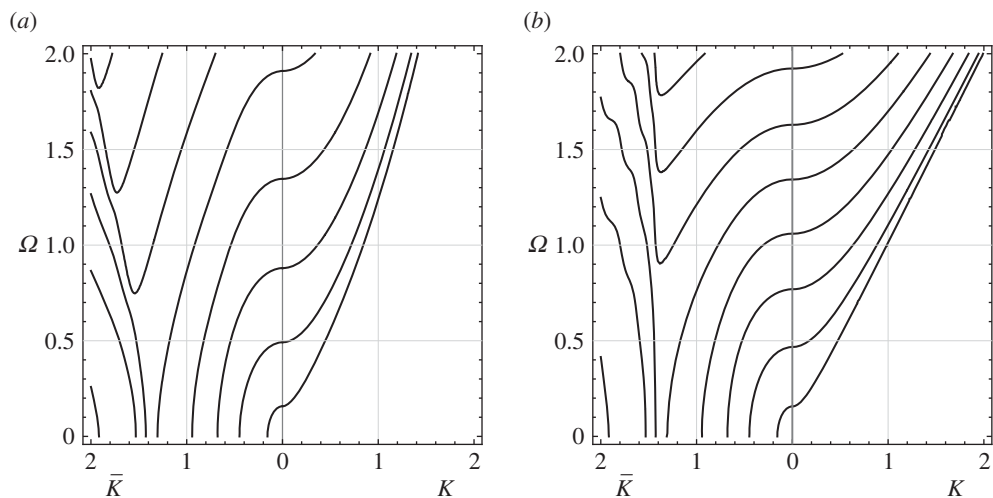
Figure 17. Frequency spectrum for antisymmetric antiplane Rayleigh–Lamb waves ($\eta = 0.1$, $H = 10$) with (a)$\ell_0 = 0.1$ and (b) $\ell_0 = \ell_{0cr}$.
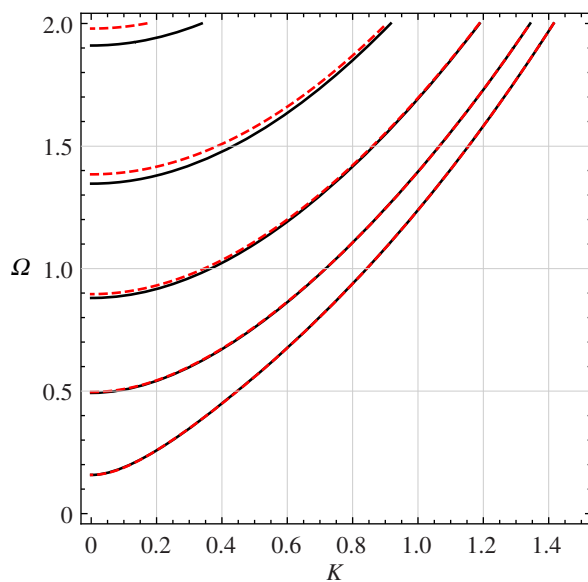

Figure 18. Antisymmetric antiplane RL waves (solid, black) and odd SH partial waves (dashed, red) frequency spectrum ($\eta = 0.1$, $\ell_0 = 0.1$, $H = 10$). All branches asymptote to bulk shear waves. (Online version in colour.)

For $\Omega \ll 1$, we have $\Theta \sim \ell_{0cr}$ and $\delta \sim \delta_{cr}$, whence $\delta/\Theta = \Omega$ and equation (4.8) gives

$$\frac{\Omega^3}{2\sqrt{2}} \tan (H\Omega) = \tanh \left(\sqrt{2}H \right), \tag{4.11}$$

that, as expected, reduces to (4.9) when $H \ll 1$. Conversely, when $H \gg 1$, we have

$$\Omega_1^* \approx \frac{\pi}{2H}, \qquad \delta^* \approx \frac{\pi}{2\sqrt{2}H},$$
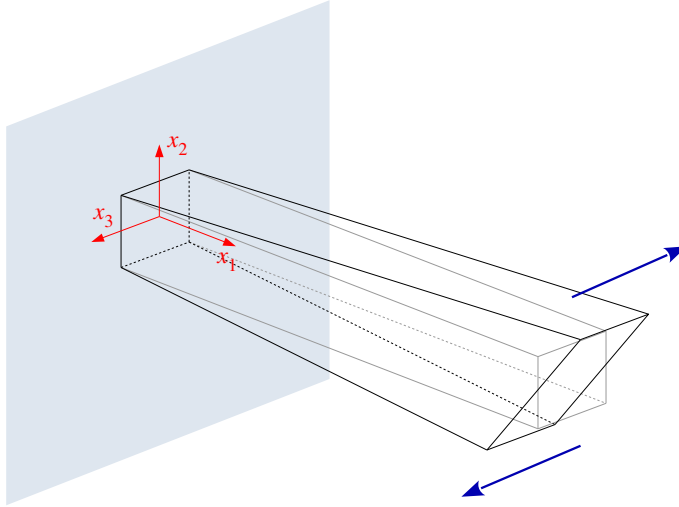
Figure 19. Antiplane antisymmetric (about the mid-plane $x_2 = 0$) vibrations of a thin beam-plate made of CS elastic material (for the sake of clarity, in this picture an element of finite thickness along x_3 is shown). Since antiplane vibrations are dealt with, any unit cross-section deforms from rectangular to rhombic, while remaining in the same (x_2, x_3) plane. (Online version in colour.)

that is exactly the situation depicted in figure 18. For the first cut-off (4.9), we get the eigenform

$$w(\xi_2) = o_1 \sin(\xi_2) + o_2 \sinh(\xi_2). \tag{4.12}$$

The thin-plate limit of the dispersion relation (4.1) gives, to leading order in H,

$$d_{ot}(\kappa, \Omega) = (1 + \delta^2)\left(-2(1 + \eta)\kappa^2 + \delta^2 - \delta^{*2}\right), \tag{4.13}$$

that, to leading order in the LWLF approximation, provides the cut-off approximation (4.9). When $\Omega - \Omega^* \ll 1$, we have the expansion

$$\delta^2 - \delta^{*2} = \sqrt{2}\ell_0^3(\Omega^2 - \Omega^{*2}) = \sqrt{2}\ell_0^3\Omega^2 - \sqrt{2}\ell_0 \ll 1,$$

whence we obtain the consistent differential model

$$\frac{1+\eta}{\sqrt{2}\ell_0^3} \frac{\partial^2 W}{\partial x_1^2} - \frac{1}{c_s^2} \frac{\partial^2 W}{\partial t^2} + \frac{1}{\ell_d^2} W = 0. \tag{4.14}$$

The same PDE governs longitudinal (or torsional) vibrations of a beam with distributed elastic restraints. However, it should be pointed out that these elastic restraints possess negative elastic constant. This equation describes the lowest antiplane antisymmetric mode for a beam made of CS material, as in figure 19. For this model, rotational inertia appears in the first and last terms.

The equivalent model in CE may be obtained letting $\ell \to 0$, whence $\Omega^* = \ell/\ell_d \to 0$ and cut-off vanishes. Then, in the LWLF regime, equation (4.13) is dominated by the δ^* term, that is $O(1)$, whence we get the trivial solution, which means that no lowest mode antisymmetric antiplane vibrations are supported. When considering the case $\eta = -1$, that corresponds to no characteristic length in torsion, the first term of (4.14) drops out and we are left with a simple ODE which warrants that solutions have an exponential form in time

$$W(\xi_1, t) = W_1(\xi_1) \exp\left(\frac{c_s}{\ell_d}t\right) + W_2(\xi_1) \exp\left(-\frac{c_s}{\ell_d}t\right).$$

Therefore, within this model, we cannot have proper vibrating antisymmetric LWLF modes either.

5. Conclusion

For an elastic theory to support Rayleigh waves, there needs to exist a form of mode conversion from travelling to inhomogeneous (surface) waves upon reflection at a free surface. Besides, this mechanism is required to stand right at grazing incidence. For instance, it may happen beyond a certain critical angle of incidence, like in sagittal plane propagation of SV waves within CE, or, as in antiplane motion for CS materials, the inhomogeneous wave may appear for all incident angles. Consequently, only one family of SV Rayleigh waves is supported in CE, for no mechanism of mode conversion exists for P and SH waves to trigger inhomogeneous waves. By the same reasons, SH Rayleigh waves cannot be sustained in CS materials when $\eta = 0$, because then mode conversion ceases to stand right at grazing incidence.

In CS materials, a novel 'reflection' mechanism occurs, according to which a bulk standing wave acts upon a surface, it is 'reflected' in its likeness (still a standing wave) and simultaneously triggers a Rayleigh-like wave that travels *away from*, not along, the surface, with phase speed lower than that of bulk shear waves. Upon approaching the grazing condition, this displacement field may be expanded in terms of the emergence angle to yield precisely the Rayleigh-like wave expressed by the purely imaginary zero of the Rayleigh function. It is exactly this wave that is found in [6] radiating from the tip of a semi-infinite crack under dynamic loadings. It is pointed out that no Rayleigh-like wave is supported in CE, for no evanescent bulk mode exists. This wave is not a leaky wave in the classical sense, for it is travelling away from the surface (while standing along the surface), with speed lower than that of shear bulk waves. Therefore, in general, complex roots of the Rayleigh functions are not expressions of leaky waves. The same result holds true for the third root of the Rayleigh function, which appears for a restricted set of material parameters and represents a attenuating/exploding travelling wave in any direction. Yet, this root differs from the other two (i.e. the real and the purely imaginary root) in that it is located far from either branch-points expressing bulk waves. Consequently, we suggest a classification of the Rayleigh function zeros according to whether they sit in the neighbourhood of or far from a branch-point. In the former case they correspond to Rayleigh, Rayleigh-like or leaky waves and represent a perturbation of the neighbouring bulk wave. In the latter case, they are waves attenuating/exploding in every direction.

Moving to guided propagation in a plate, we determine a generalized set of Mindlin's boundary conditions for identifying partial modes. Under such conditions, wave reflection occurs in the absence of mode conversion, equally so for travelling and for standing modes. Only one family of travelling partial modes exists in CS materials, along with a family of standing modes. As a result, travelling Rayleigh–Lamb modes are simply guided by and asymptote to travelling partial modes, with the exception of the first even mode (the lowest mode) that asymptotes to the Rayleigh wave speed. Hence, just like in plane-strain elasticity, lowest mode SWHF perturbations are guided by one boundary, as in a half-plane [39]. Conversely, standing Rayleigh–Lamb modes are more complicated, for they are obtained by interference of two families of partial waves. When considering travelling modes, a thin-plate approximation gives the equivalent one-dimensional model for describing lowest symmetric and antisymmetric modes. Such approximated models should be used when building a theory of antiplane vibrations of thin beam-plates made of CS material [38,40].

References

1. Strutt W. 1885 On waves propagated along the plane surface of an elastic solid. *Proc. Lond. Math. Soc.* **1**, 4–11.
2. Ewing W, Jardetzky W, Press F. 1957 *Elastic waves in layered media*. McGraw-Hill Series in the Geological Science. New York, NY: McGraw Hill Book Company Inc.
3. Love A. 1911 *Some problems of geodynamics*. Cambridge, UK: Cambridge University Press.
4. Gourgiotis P, Georgiadis H. 2015 Torsional and SH surface waves in an isotropic and homogenous elastic half-space characterized by the Toupin–Mindlin gradient theory. *Int. J. Solids Struct.* **62**, 217–228. (doi:10.1016/j.ijsolstr.2015.02.032)
5. Morini L, Piccolroaz A, Mishuris G. 2014 Remarks on the energy release rate for an antiplane moving crack in couple stress elasticity. *Int. J. Solids Struct.* **51**, 3087–3100. (doi:10.1016/j.ijsolstr.2014.05.005)
6. Nobili A, Radi E, Vellender A. 2019 Diffraction of antiplane shear waves and stress concentration in a cracked couple stress elastic material with micro inertia. *J. Mech. Phys. Solids* **124**, 663–680. (doi:10.1016/j.jmps.2018.11.013)
7. Maugin G. 1988 Shear horizontal surface acoustic waves on solids. In *Recent Developments in Surface Acoustic Waves: Proc. of European Mechanics Colloqium* 226 (eds DF Parker, GA Maugin), pp. 158–172. Berlin/Heidelberg, Germany: Springer-Verlag.
8. Collet B, Destrade M, Maugin G. 2006 Bleustein–Gulyaev waves in some functionally graded materials. *Eur. J. Mech. A Solids* **25**, 695–706. (doi:10.1016/j.euromechsol.2006.01.007)
9. Mindlin R, Tiersten H. 1962 Effects of couple-stresses in linear elasticity. *Arch. Ration. Mech. Anal.* **11**, 415–448. (doi:10.1007/BF00253946)
10. Toupin R. 1962 Elastic materials with couple-stresses. *Arch. Ration. Mech. Anal.* **11**, 385–414. (doi:10.1007/BF00253945)
11. Koiter W. 1964 Couple-stress in the theory of elasticity. In *Proc. K. Ned. Akad. Wet*, vol. 67, pp. 17–44. North Holland Pub.
12. Ottosen NS, Ristinmaa M, Ljung C. 2000 Rayleigh waves obtained by the indeterminate couple-stress theory. *Eur. J. Mech. A Solids* **19**, 929–947. (doi:10.1016/S0997-7538(00)00201-1)
13. Radi E. 2008 On the effects of characteristic lengths in bending and torsion on Mode III crack in couple stress elasticity. *Int. J. Solids Struct.* **45**, 3033–3058. (doi:10.1016/j.ijsolstr.2008.01.010)
14. Itou S. 2013 Effect of couple-stresses on the stress intensity factors for a crack in an infinite elastic strip under tension. *Eur. J. Mech. A Solids* **42**, 335–343. (doi:10.1016/j.euromechsol.2013.07.004)
15. Graff KF, Pao YH. 1967 The effects of couple-stresses on the propagation and reflection of plane waves in an elastic half-space. *J. Sound Vib.* **6**, 217–229. (doi:10.1016/0022-460X(67)90229-5)
16. Gourgiotis P, Georgiadis H, Neocleous I. 2013 On the reflection of waves in half-spaces of microstructured materials governed by dipolar gradient elasticity. *Wave Motion* **50**, 437–455. (doi:10.1016/j.wavemoti.2012.10.004)
17. Sengupta P, Ghosh B. 1974 Effect of couple-stresses on the propagation of waves in an elastic layer. *Pure Appl. Geophys.* **112**, 331–338. (doi:10.1007/BF00876144)
18. Ghodrati B, Yaghootian A, Ghanbar Zadeh A, Mohammad-Sedighi H. 2018 Lamb wave extraction of dispersion curves in micro/nano-plates using couple stress theories. *Waves Random Complex Media* **28**, 15–34. (doi:10.1080/17455030.2017.1308582)
19. Georgiadis H, Velgaki E. 2003 High-frequency Rayleigh waves in materials with micro-structure and couple-stress effects. *Int. J. Solids Struct.* **40**, 2501–2520. (doi:10.1016/S0020-7683(03)00054-4)
20. Mishuris G, Piccolroaz A, Radi E. 2012 Steady-state propagation of a Mode III crack in couple stress elastic materials. *Int. J. Eng. Sci.* **61**, 112–128. (doi:10.1016/j.ijengsci.2012.06.015)
21. Shodja H, Goodarzi A, Delfani M, Haftbaradaran H. 2015 Scattering of an anti-plane shear wave by an embedded cylindrical micro-/nano-fiber within couple stress theory with micro inertia. *Int. J. Solids Struct.* **58**, 73–90. (doi:10.1016/j.ijsolstr.2014.12.020)
22. Lakes R. 1986 Experimental microelasticity of two porous solids. *Int. J. Solids Struct.* **22**, 55–63. (doi:10.1016/0020-7683(86)90103-4)
23. Nakamura S, Lakes R. 1995 Finite element analysis of Saint-Venant end effects in micropolar elastic solids. *Eng. Comput.* **12**, 571–587. (doi:10.1108/02644409510799785)
24. Zhang L, Huang Y, Chen J, Hwang K. 1998 The mode III full-field solution in elastic materials with strain gradient effects. *Int. J. Fract.* **92**, 325–348. (doi:10.1023/A:1007552621307)

25. Yang F, Chong A, Lam D, Tong P. 2002 Couple stress based strain gradient theory for elasticity. *Int. J. Solids Struct.* **39**, 2731–2743. (doi:10.1016/S0020-7683(02)00152-X)
26. Zisis T. 2018 Anti-plane loading of microstructured materials in the context of couple stress theory of elasticity: half-planes and layers. *Arch. Appl. Mech.* **88**, 97–110. (doi:10.1007/s00419-017-1277-2)
27. Pujol J. 2003 *Elastic wave propagation and generation in seismology*. Cambridge, UK: Cambridge University Press.
28. Solie L, Auld B. 1973 Elastic waves in free anisotropic plates. *J. Acoust. Soc. Am.* **54**, 50–65. (doi:10.1121/1.1913575)
29. Graff KF. 1991 *Wave motion in elastic solids*. New York, NY: Dover Publications Inc.
30. Achenbach J. 1984 *Wave propagation in elastic solids*. Applied Mathematics and Mechanics, vol. 16. Amsterdam, The Netherlands: North-Holland, Elsevier.
31. Mindlin R. 1960 Waves and vibrations in isotropic, elastic plates. In *Structural Mechanics: Proc. of the First Symp. on Naval Structural Mechanics, Stanford University, CA* (eds JM Goodier, NJ Hoff), pp. 199–232. Oxford, UK/New York, NY: Pergamon Press.
32. Miklowitz J. 2012 *The theory of elastic waves and waveguides*. North-Holland Series in Applied Mathematics, vol. 22. Amsterdam, The Netherlands: Elsevier.
33. Goodier J, Bishop R. 1952 A note on critical reflections of elastic waves at free surfaces. *J. Appl. Phys.* **23**, 124–126. (doi:10.1063/1.1701956)
34. Schröder C, Scott Jr WR. 2001 On the complex conjugate roots of the Rayleigh equation: the leaky surface wave. *J. Acoust. Soc. Am.* **110**, 2867–2877. (doi:10.1121/1.1419085)
35. Nobili A, Radi E, Lanzoni L. 2017 Flexural edge waves generated by steady-state propagation of a loaded rectilinear crack in an elastically supported thin plate. *Proc. R. Soc. A* **473**, 20170265. (doi:10.1098/rspa.2017.0265)
36. Noble B. 1958 *Methods based on the Wiener-Hopf technique for the solution of partial differential equations*. International Series of Monographs on Pure and Applied Mathematics, vol. 7. New York, NY: Pergamon Press.
37. Erbaş B, Kaplunov J, Nobili A, Kılıç G. 2018 Dispersion of elastic waves in a layer interacting with a Winkler foundation. *J. Acoust. Soc. Am.* **144**, 2918–2925. (doi:10.1121/1.5079640)
38. Engelbrecht J, Berezovski A, Pastrone F, Braun M. 2005 Waves in microstructured materials and dispersion. *Philos. Mag.* **85**, 4127–4141. (doi:10.1080/14786430500362769)
39. Nobili A, Prikazchikov DA. 2018 Explicit formulation for the Rayleigh wave field induced by surface stresses in an orthorhombic half-plane. *Eur. J. Mech. A Solids* **70**, 86–94. (doi:10.1016/j.euromechsol.2018.01.012)
40. Kaplunov J, Zakharov A, Prikazchikov D. 2006 Explicit models for elastic and piezoelastic surface waves. *IMA J. Appl. Math.* **71**, 768–782. (doi:10.1093/imamat/hxl012)